

# Topological segregation of stress sensors along the gut crypt–villus axis

<https://doi.org/10.1038/s41586-024-08581-9>

Received: 16 April 2024

Accepted: 27 December 2024

Published online: 12 February 2025

 Check for updates

Kouki K. Touhara<sup>1</sup>, Nathan D. Rossen<sup>1,2,8</sup>, Fei Deng<sup>3,4,8</sup>, Joel Castro<sup>5,6,8</sup>, Andrea M. Harrington<sup>5,6</sup>, Tiffany Chu<sup>7</sup>, Sonia Garcia-Caraballo<sup>5,6</sup>, Mariana Brizuela<sup>5,6</sup>, Tracey O'Donnell<sup>5</sup>, Jinhao Xu<sup>1</sup>, Onur Cil<sup>7</sup>, Stuart M. Brierley<sup>5,6</sup>, Yulong Li<sup>3,4</sup> & David Julius<sup>1</sup>

The crypt–villus structure of the small intestine serves as an essential protective barrier. The integrity of this barrier is monitored by the complex sensory system of the gut, in which serotonergic enterochromaffin (EC) cells play an important part<sup>1,2</sup>. These rare sensory epithelial cells surveil the mucosal environment for luminal stimuli and transmit signals both within and outside the gut<sup>3–6</sup>. However, whether EC cells in crypts and villi detect different stimuli or produce distinct physiological responses is unknown. Here we address these questions by developing a reporter mouse model to quantitatively measure the release and propagation of serotonin from EC cells in live intestines. Crypt EC cells exhibit a tonic low-level mode that activates epithelial serotonin 5-HT<sub>4</sub> receptors to modulate basal ion secretion and a stimulus-induced high-level mode that activates 5-HT<sub>3</sub> receptors on sensory nerve fibres. Both these modes can be initiated by the irritant receptor TRPA1, which is confined to crypt EC cells. The activation of TRPA1 by luminal irritants is enhanced when the protective mucus layer is compromised. Villus EC cells also signal damage through a distinct mechanism, whereby oxidative stress activates TRPM2 channels, which leads to the release of both serotonin and ATP and consequent excitation of sensory nerve fibres. This topological segregation of EC cell functionality along the mucosal architecture constitutes a mechanism for the surveillance, maintenance and protection of gut integrity under diverse physiological conditions.

The gastrointestinal (GI) tract is equipped with a complex sensory system that detects the state of the gut mucosa and transmits signals within and outside this visceral organ. The first line of stimulus detection is mediated by enteroendocrine cells, which are rare specialized sensory cells within the gut epithelium that release hormones and neurotransmitters in response to endogenous and exogenous stimuli<sup>7</sup>. EC cells are a subclass of excitable enteroendocrine cells that release serotonin (5-HT) in response to bacterial metabolites, neurotransmitters, peptide hormones, interleukins, and ingested or endogenous irritants<sup>1–6,8</sup>. EC cells also show spontaneous (basal) activity, for which an underlying mechanism or physiological role remains unknown<sup>4,9</sup>.

Several serotonin receptor subtypes are present in the gut<sup>2</sup>, including ionotropic 5-HT<sub>3</sub> and metabotropic 5-HT<sub>4</sub> receptors, which have been pharmacologically targeted to treat GI dysregulation associated with diarrhoea or constipation<sup>2,10</sup>. EC cells transduce signals to afferent sensory nerve fibres within the mucosa that express 5-HT<sub>3</sub> receptors, which are excitatory ion channels activated by relatively high (micromolar) concentrations of serotonin<sup>1,2,11</sup>. This serotonergic EC cell–sensory neuron circuit modulates a range of processes, including GI motility, secretion, nausea and pain<sup>2,12,13</sup>. By contrast, G protein-coupled 5-HT<sub>4</sub> receptors on intestinal epithelial cells are activated by relatively low

(nanomolar) levels of serotonin, which leads to enhanced ion secretion<sup>14,15</sup>. This latter process has a crucial role in the maintenance of fluid balance in the gut to aid digestion and to protect the intestinal lining by supporting the formation of a mucus barrier<sup>16</sup>. However, we do not fully understand the mechanism by which EC cells achieve the thousand-fold difference in serotonin concentration required to differentially activate 5-HT<sub>3</sub> or 5-HT<sub>4</sub> receptors. Moreover, whether or how this mechanism relates to the excitability status of EC cells under distinct physiological circumstances is unclear.

Such potential differential actions raise interesting questions about the temporal and spatial nature of serotonergic signalling in the intestine and how this relates to the arrangement of crypts and villi that define the complex architecture of the gut. Crypts are small invaginations within the epithelium that house stem cells. These cells are vulnerable to microorganisms and irritants and are therefore protected by antimicrobial peptides and a thick layer of mucus<sup>17</sup>. Villi are long finger-like projections that extend from crypts towards the lumen and are more directly exposed to contents of the lumen. EC cells change their molecular identity as they migrate from crypts to villi. For example, two distinct members of the transient receptor potential (TRP) ion channel family that sense environmental stress are segregated

<sup>1</sup>Department of Physiology, University of California San Francisco, San Francisco, CA, USA. <sup>2</sup>Tetrad Graduate Program, University of California San Francisco, San Francisco, CA, USA. <sup>3</sup>State Key Laboratory of Membrane Biology, New Cornerstone Science Laboratory, School of Life Sciences, Peking University, Beijing, China. <sup>4</sup>PKU-IDG/McGovern Institute for Brain Research, Beijing, China. <sup>5</sup>Visceral Pain Research Group, Hopwood Centre for Neurobiology, South Australian Health and Medical Research Institute (SAHMRI), Adelaide, South Australia, Australia. <sup>6</sup>Faculty of Health and Medical Sciences, University of Adelaide, Adelaide, South Australia, Australia. <sup>7</sup>Department of Pediatrics, University of California San Francisco, San Francisco, CA, USA. <sup>8</sup>These authors contributed equally: Nathan D. Rossen, Fei Deng, Joel Castro. ✉e-mail: Koki.Touhara@ucsf.edu; Stuart.Brierley@sahmri.com; yulongli@pku.edu.cn; David.Julius@ucsf.edu

within the crypt–villus axis. TRPA1 (also known as the wasabi receptor), which detects reactive electrophilic irritants, is located predominantly in crypts, whereas TRPM2, which senses intracellular ADP ribose as a measure of oxidative stress, is found mostly in villi<sup>18–20</sup>. An important question to answer is whether EC cells in these different tissue compartments respond to distinct stimuli to produce differential physiological actions and how this relates to the distribution of 5-HT receptor subtypes and the dynamics of transmitter release within the crypt–villus architecture. Addressing these questions requires the development of new quantitative approaches for analysing signalling in a complex organ structure with spatial and temporal resolution, as has been advocated for the gut<sup>21</sup>.

In this study, we describe a mouse model that enables direct observation of serotonin release and propagation within the intact crypt–villus architecture. Using this system, we determine how differential release of serotonin from EC cells promotes distinct physiological responses. We also investigate how crypt and villus EC cells use different TRP channels and transmitters to detect and transduce exogenous or endogenous stress signals within and beyond the gut.

### Spatiotemporal dynamics of gut serotonin

To monitor real-time release and propagation of serotonin within the crypt–villus architecture, we set out to develop a mouse model in which genetically encoded G protein-coupled receptor (GPCR)-activation-based serotonin sensors are expressed in the intestinal epithelium<sup>22,23</sup>. gGRAB<sub>5-HT3.0</sub> is an improved sensor for which fluorescence intensity increases after it binds to serotonin<sup>23</sup> (Extended Data Fig. 1a). We developed a transgenic mouse line that expresses gGRAB<sub>5-HT3.0</sub> and a red-shifted Ca<sup>2+</sup> indicator, jRGECO1a, after exposure to Cre recombinase (Extended Data Fig. 1b). Crossing this reporter line to *Vil1*<sup>cre</sup> mice resulted in the expression of gGRAB<sub>5-HT3.0</sub> and jRGECO1a in intestinal epithelial cells (Extended Data Fig. 1c), which facilitated the visualization of the release and propagation of serotonin within the gut using fluorescence microscopy. Note that expression levels of gGRAB<sub>5-HT3.0</sub> and jRGECO1a are slightly higher in villi compared to crypts (Extended Data Fig. 1d) and decrease progressively in the proximal and distal colon, a result consistent with the expression pattern of the *Vil1* gene<sup>24</sup> (Extended Data Fig. 1c). To visualize reporter activation, we removed a section of jejunum, flushed the luminal contents out and then dissected the tissue to create a flat sheet. We imaged the tissue from the smooth muscle side to visualize crypts or from the luminal side to observe villi. When exposed to a high K<sup>+</sup> solution, EC cells released serotonin and subsequently activated the gGRAB<sub>5-HT3.0</sub> sensor, which is expressed in both EC cells and adjacent epithelial cells within crypts and villi (Fig. 1a, b and Supplementary Videos 1 and 2). We observed that EC cells exhibit the highest gGRAB<sub>5-HT3.0</sub> fluorescence intensity in both fixed tissue and live tissue, which facilitated their identification during imaging (Fig. 1c–e).

### Two modes of serotonin release in crypts

Having established a tool to visualize serotonin release in the intact intestine, we observed a differential profile whereby tonic serotonin release was seen in crypts but not villi (Fig. 2a and Supplementary Video 3). This tonic release was similarly observed when crypts were isolated from intact tissue (Extended Data Fig. 2a). We noted that this differential activity aligned with the preferential expression of TRPA1 in crypt EC cells<sup>18–20</sup>. In situ hybridization histochemistry revealed strong *Trpa1* expression in crypts that reduced progressively from lower to upper villi (Extended Data Fig. 2b). This result was further supported by re-analysis of a published single-cell RNA sequencing (scRNA-seq) dataset<sup>20</sup>, which revealed a gradient of *Trpa1* expression, with the highest levels in crypt EC cells and progressively lower expression towards villi (Extended Data Fig. 2c). To functionally validate

these expression data, we assessed serotonin release from dissociated crypts and upper villi after stimulation with the TRPA1 agonist allyl isothiocyanate (AITC). Consistent with the observed gradient of *Trpa1* expression, AITC-induced serotonin release was detected in dissociated crypts but not in similarly dissociated upper villi (Extended Data Fig. 2d). To determine whether TRPA1 contributes to tonic serotonin release in crypt EC cells, we examined intestinal organoids derived from *Tac1*<sup>Cre</sup>; *Polr2a*<sup>(GCaMP5g-IRES-tdTomato)</sup> mice, which express the Ca<sup>2+</sup> indicator GCaMP5g and tdTomato specifically in EC cells (Extended Data Fig. 2e). In these organoids, which replicate crypt features<sup>18</sup>, a TRPA1 antagonist, A967079 (A96), reduced the spontaneous activity of EC cells (Fig. 2b). We consistently observed A96-sensitive spontaneous TRPA1 channel openings in single-cell voltage-clamp recordings from EC cells (Extended Data Fig. 2f) and found that A96-sensitive spontaneous membrane depolarizations drove repeated action potentials (Extended Data Fig. 2g). Moreover, spontaneous calcium flux in EC cells was inhibited by tetrodotoxin, a voltage-gated sodium channel (Na<sub>v</sub>) blocker (Extended Data Fig. 2h). Taken together, these results demonstrate that low levels of TRPA1 channel opening are sufficient to drive Na<sub>v</sub>-dependent action potentials, which lead to tonic serotonin release from crypt EC cells.

The normalized gGRAB<sub>5-HT3.0</sub> sensor response suggested that tonic serotonin release is only a fraction of stimulated release (Fig. 2c). To verify this observation, we quantitatively compared tonic and AITC-induced serotonin release from crypt EC cells in intestinal organoids. For this experiment, we used the low-affinity serotonin sensor gGRAB<sub>5-HT2m</sub>, which is more suitable for measuring serotonin within the micromolar range<sup>23</sup>. We positioned a human embryonic kidney (HEK293) cell expressing gGRAB<sub>5-HT2m</sub> adjacent to (5 μm away from) an EC cell in *Tac1*<sup>Cre</sup>; *Polr2a*<sup>(GCaMP5g-IRES-tdTomato)</sup> organoids. This enabled us to monitor spontaneous and AITC-induced calcium signals in EC cells while simultaneously monitoring serotonin release with the juxtaposed biosensor cell (Fig. 2d). At the end of each recording, we applied a maximally effective concentration of serotonin to fully activate the gGRAB<sub>5-HT2m</sub> sensor. This normalization step enabled us to estimate the local concentration of released serotonin based on the dose–response curve of the sensor (Extended Data Fig. 2i). We observed a substantially lower GCaMP signal during the tonic phase than with the AITC-stimulated phase (Fig. 2e), with a corresponding difference in the level of released serotonin (Fig. 2f). Specifically, tonic serotonin release remained at a minimal level such that the normalized gGRAB<sub>5-HT2m</sub> amplitude exceeded 0.63 (corresponding to 1 μM serotonin) in only 1 out of 8 cells examined. Conversely, for AITC-stimulated release, the normalized gGRAB<sub>5-HT2m</sub> amplitude exceeded 0.63 in 6 out of 9 cells evaluated.

If tonic serotonin release is in the nanomolar range, then basal EC cell activity should predominantly activate high-affinity metabotropic 5-HT receptors, whereas stimulated EC cells should activate both metabotropic and lower affinity ionotropic receptors. To test this hypothesis, we first monitored GCaMP signals in EC cells within organoids to observe their activity while simultaneously measuring whole-cell currents in neighbouring HEK293 biosensor cells expressing ionotropic 5-HT<sub>3</sub> receptors<sup>11</sup> (Fig. 2g). As expected, peak 5-HT<sub>3</sub> currents were substantially smaller during tonic serotonin release than with AITC-stimulated release (Fig. 2g–i). This result is consistent with the idea that EC cells activate ionotropic 5-HT<sub>3</sub> receptors most strongly when stimulated by agonists.

By contrast, tonic serotonin release should activate 5-HT<sub>4</sub> or 5-HT<sub>2</sub> metabotropic receptor subtypes, which exhibit nanomolar sensitivity to serotonin<sup>14,25</sup>. To test this prediction, we developed a biosensor in which HEK293 cells express both Gq-coupled 5-HT<sub>2A</sub> receptors and GCaMP8m. When activated, 5-HT<sub>2A</sub> receptors promote endoplasmic-reticulum-stored Ca<sup>2+</sup> release, which results in increased GCaMP8m fluorescence. Notably, low nanomolar concentrations of serotonin repeatedly activated this biosensor without apparent desensitization

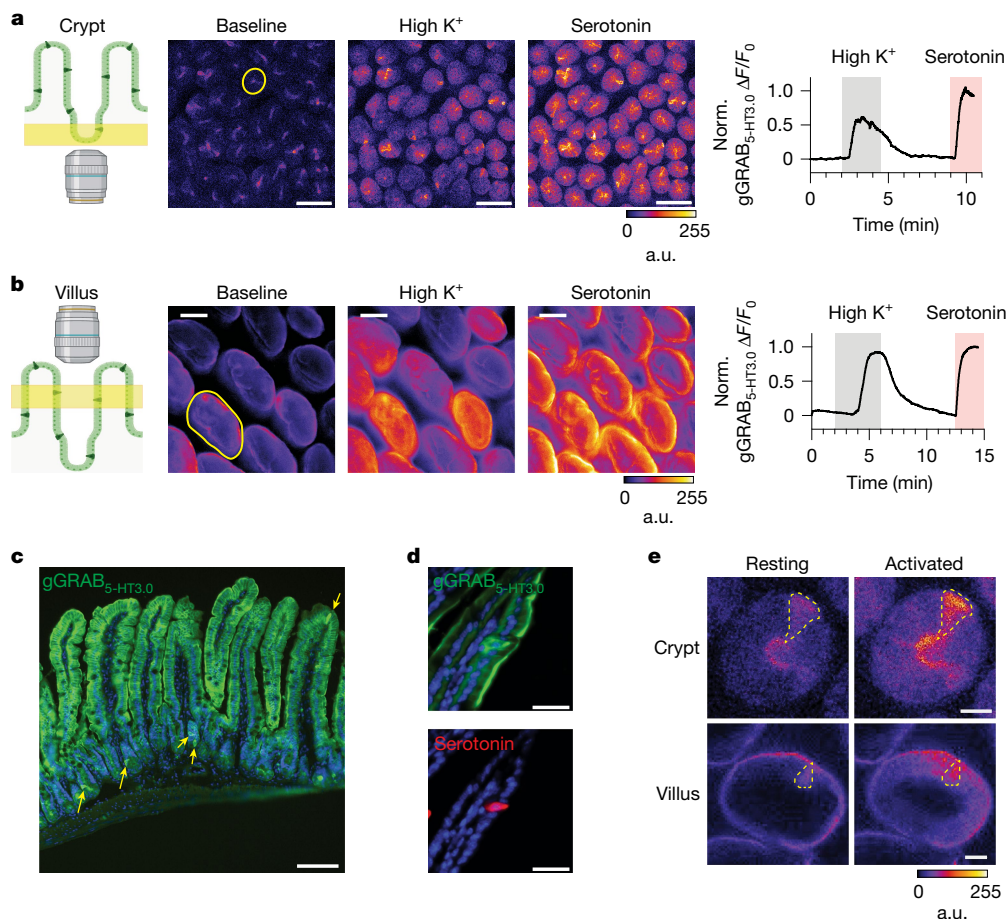


**Fig. 1 | Live imaging of EC-cell-derived serotonin in the intact crypt–villus architecture.** **a,b**, Examples of gGRAB<sub>5-HT3.0</sub> imaging (left) and quantification in crypts (**a**) and villi (**b**). Serotonin release was stimulated by application of high K<sup>+</sup> (70 mM KCl). gGRAB<sub>5-HT3.0</sub> was fully activated with 20 μM serotonin at the end of recordings so that change in fluorescence ( $\Delta F/F_0$ ) values could be normalized (Norm.). The graphs represent the averaged signal from a single crypt or villus, with yellow circles in the images indicating the region of interest (ROI) used for plotting. **c**, Expression pattern of gGRAB<sub>5-HT3.0</sub> in the small

intestine. gGRAB<sub>5-HT3.0</sub> was immunostained with an anti-GFP antibody. Arrows indicate EC cells in crypts and villi. **d**, The immunofluorescence intensity of gGRAB<sub>5-HT3.0</sub> is higher in EC cells compared with other epithelial cells. **e**, Examples of live gGRAB<sub>5-HT3.0</sub> imaging in crypt EC (top) and villus EC (bottom) cells after high K<sup>+</sup> activation. EC cells are outlined with dashed yellow lines. Scale bars, 100 μm (**a–c**), 30 μm (**d**) or 20 μm (**e**). All experiments were repeated at least ten times with similar results. a.u., arbitrary units. Illustrations in **a** and **b** were created using BioRender (<https://biorender.com>).

(Extended Data Fig. 2j). Despite observing a stronger calcium response in EC cells during the AITC-stimulated phase, peak 5-HT<sub>2A</sub> biosensor responses during tonic and AITC-stimulated release were equivalent (Fig. 2j–l). Taken together, the results from the gGRAB<sub>5-HT2m</sub>, 5-HT<sub>3</sub> and 5-HT<sub>2A</sub> biosensor experiments are in agreement and suggest that tonic nanomolar serotonin activates metabotropic, rather than ionotropic, 5-HT receptors. Conversely, when crypt EC cells are stimulated by electrophiles (or other agonists), they release micromolar concentrations of serotonin, which leads to the activation of both metabotropic and ionotropic 5-HT receptors.

### 5-HT receptors in the crypt–villus axis

We next examined the physiological consequences of tonic serotonin release compared with stimulated release in crypts. We focused on 5-HT<sub>3</sub> and 5-HT<sub>4</sub> subtypes as the most relevant targets in the intestine<sup>2,10</sup>. We first investigated the distribution of 5-HT<sub>4</sub> receptors, which are known to stimulate epithelial chloride secretion to influence the rate of fluid transfer into the intestinal lumen<sup>15</sup>. An analysis of published scRNA-seq datasets revealed that 5-HT<sub>4</sub> receptors are expressed exclusively within crypts, primarily in progenitor cells and with slightly lower expression in Paneth cells (Extended Data Fig. 3a). Consistent with

this finding, in situ hybridization histochemistry showed that 5-HT<sub>4</sub> transcripts (*Htr4*) are expressed in crypts (but not villi) (Fig. 3a,b), specifically by *Olfm4*-positive progenitor cells and LYZ-positive Paneth cells (Extended Data Fig. 3b). We therefore predicted that tonically released serotonin from crypt EC cells would activate these receptors. To demonstrate the communication between EC cells and 5-HT<sub>4</sub> receptors in crypts, we used an Ussing chamber to measure ion secretion in ex vivo intestinal preparations. Consistent with previous findings<sup>15</sup>, bath-applied serotonin stimulated ion secretion in a 5-HT<sub>4</sub>-dependent manner (Fig. 3c and Extended Data Fig. 3c). To specifically activate EC cells, we used a previously established mouse line, in which deschloroclozapine (DCZ) triggers serotonin release from EC cells that selectively express excitatory DREADD receptors<sup>13</sup>. Application of DCZ stimulated ion secretion, a result that confirmed the presence of a functional communication axis between EC cells and 5-HT<sub>4</sub> receptor-expressing crypt cells (Fig. 3d and Extended Data Fig. 3c).

In light of these results, we examined the contribution of tonic serotonin release to basal ion secretion using intestinal organoids. Activation of the stimulatory G protein (G<sub>s</sub>) pathway is known to induce fluid secretion, which in turn leads to organoid swelling<sup>26</sup>. Acute exposure to serotonin produced organoid swelling in a 5-HT<sub>4</sub> (but not 5-HT<sub>3</sub>)-dependent manner (Fig. 3e). Furthermore, a reduction in basal swelling

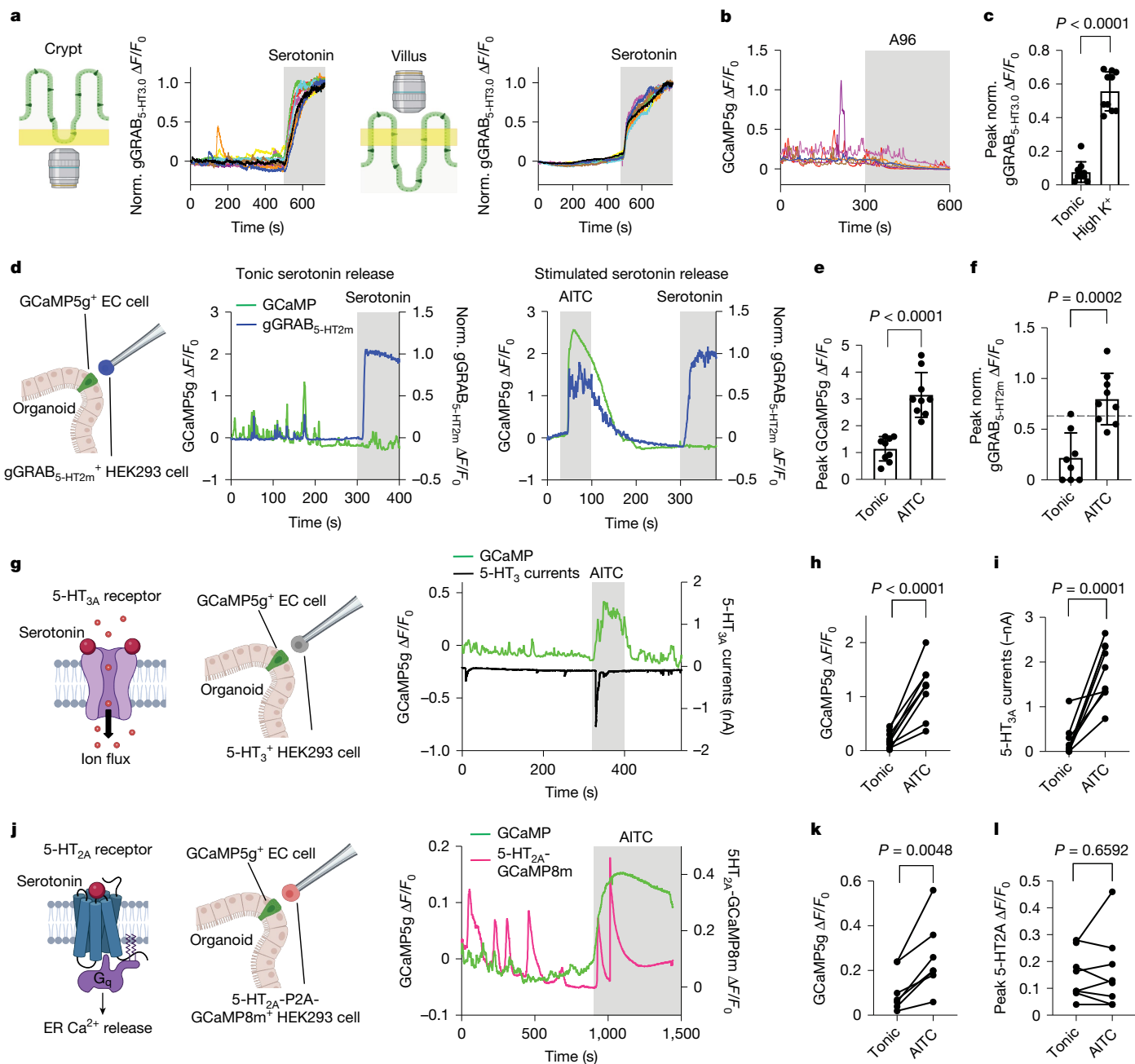


**Fig. 2 | Crypt EC cells show two modes of serotonin release that depend on TRPA1.** **a**, Basal serotonin release in crypts (left) and villi (right) in ex vivo preparations. gGRAB<sub>5-HT3.0</sub> was fully activated with 20 μM serotonin at the end of recordings for normalization. Each coloured trace represents an individual crypt or villus. **b**, A96 (10 μM), a TRPA1 antagonist, inhibits the tonic activity of crypt EC cells in intestinal organoids. **c**, Peak normalized gGRAB<sub>5-HT3.0</sub> responses within crypts were measured in ex vivo preparations during the tonic and high K<sup>+</sup> stimulated phases. Mean ± s.d., two-sided Mann–Whitney *U*-test (*n* = 10 crypts). **d**, In each experiment, a HEK293 cell expressing gGRAB<sub>5-HT2m</sub> was positioned 5 μm away from a GCaMP5g-expressing organoid EC cell. The gGRAB<sub>5-HT2m</sub> and GCaMP5g signals were simultaneously measured during tonic or AITC-stimulated activity. gGRAB<sub>5-HT2m</sub> was fully activated with 500 μM serotonin at the end of recordings for normalization. **e**, Peak GCaMP5g responses of EC cells during tonic versus AITC-stimulated activity. Mean ± s.d., two-sided Welch’s *t*-test (*n* = 8 (tonic) and 9 (AITC) cells). **f**, Peak normalized

gGRAB<sub>5-HT2m</sub> responses during tonic versus AITC-stimulated activity. The dashed line indicates a normalized gGRAB<sub>5-HT2m</sub> response of 0.63, corresponding to 1 μM serotonin. Mean ± s.d., two-sided Welch’s *t*-test (*n* = 8 (tonic) and 9 (AITC) cells). **g–i**, Single-cell patch-clamp recordings were performed on HEK293 cells positioned 5 μm away from GCaMP5g-expressing EC cells in organoids (**g**). Inward 5-HT<sub>3</sub> currents were measured while the GCaMP5g signal was recorded. Peak GCaMP5g response (**h**) and maximum inward 5-HT<sub>3</sub> currents (**i**) during tonic versus AITC-stimulated activity. Two-sided paired *t*-test (*n* = 9 cells). **j–l**, In each experiment, a HEK293 cell expressing GCaMP8m and 5-HT<sub>2A</sub> receptors was positioned 5 μm away from a GCaMP5g-expressing organoid EC cell (**j**). Peak GCaMP5g (**k**) and 5-HT<sub>2A</sub>-GCaMP8m responses (**l**) were measured during tonic and AITC-stimulated phases. Two-sided paired *t*-test (*n* = 8). ER, endoplasmic reticulum. Illustrations in **a**, **d**, **g** and **j** were created using BioRender (<https://www.biorender.com>).

was observed when organoids were incubated with a TRPA1 antagonist (A96) or a 5-HT<sub>4</sub> antagonist (RS 23597-190) (Fig. 3f). This result suggested that TRPA1-induced tonic serotonin release contributes

to organoid swelling through the activation of 5-HT<sub>4</sub> receptors. Notably, long-term exposure to A96 or RS 23597-190 did not affect overall organoid growth, a result that excluded the potential impact of these

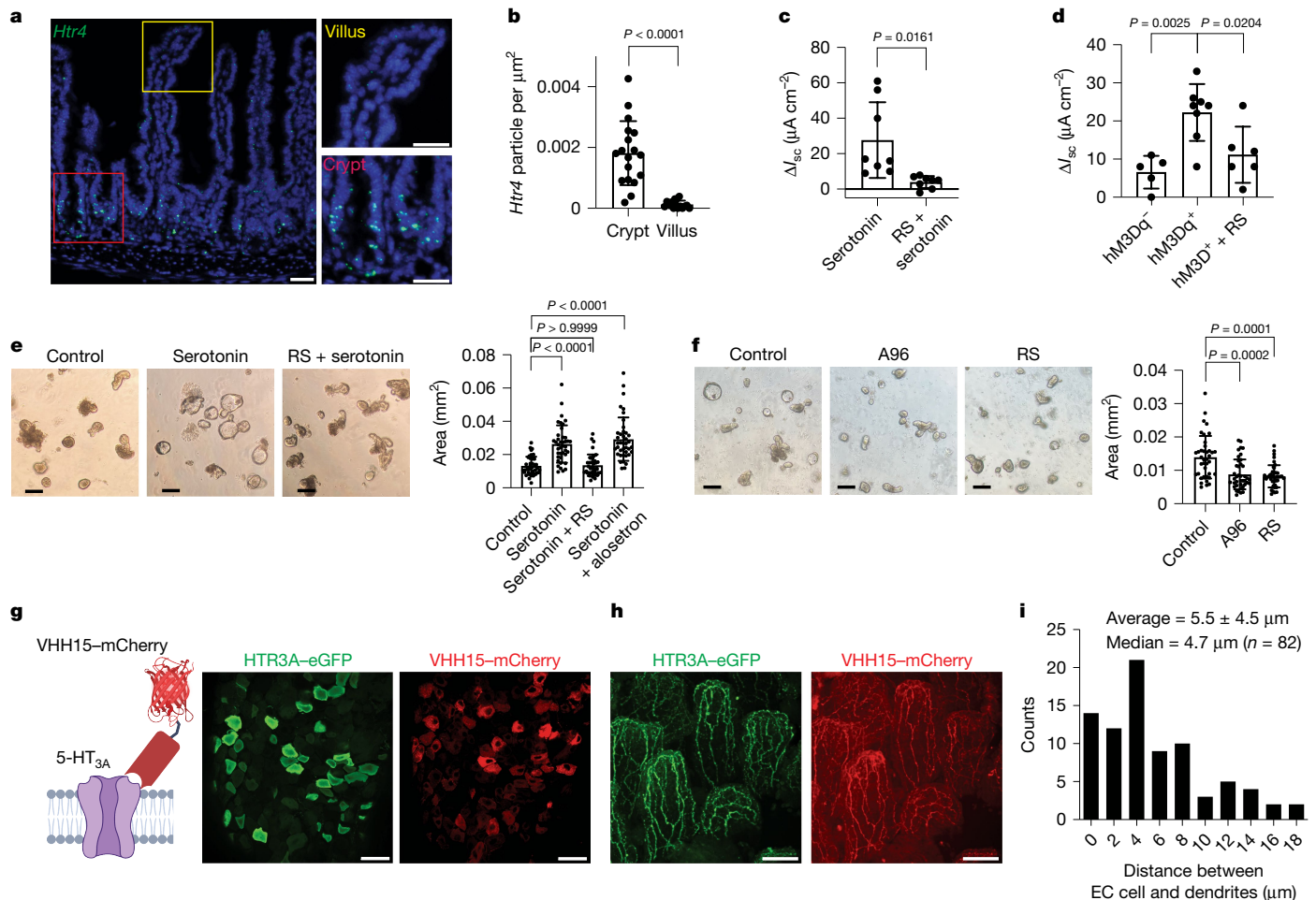


**Fig. 3 | Metabotropic and ionotropic 5-HT receptors reside in proximity to crypt EC cells.** **a**, In situ hybridization of *Htr4* in the small intestine. Magnified images of the villus (yellow) and crypt (red). **b**, Quantification of *Htr4* levels in crypts and villi. Mean  $\pm$  s.d., two-sided Welch's *t*-test ( $n = 15$  crypts and 18 villi;  $N = 2$  animals). **c**, Ion secretion in the intestine was measured using an Ussing chamber. Summary of changes in the short-circuit current ( $I_{sc}$ ) induced by 1  $\mu$ M serotonin with or without pretreatment with a 5-HT<sub>4</sub> antagonist (1  $\mu$ M RS 23597-190 (RS)). Mean  $\pm$  s.d., two-sided Welch's *t*-test ( $n = 8$  recordings). **d**, Summary of changes in the  $I_{sc}$  induced by 1  $\mu$ M DCZ in the intestine isolated from mice expressing hM3Dq receptor specifically in EC cells, with or without 1  $\mu$ M RS 23597-190. Mean  $\pm$  s.d., one-way analysis of variance (ANOVA) with Tukey's post-hoc test.  $n$  (left to right) = 5, 8 and 6 recordings. **e**, Intestinal organoids were incubated with 1  $\mu$ M serotonin with or without 10  $\mu$ M RS 23597-190 or

3  $\mu$ M alonetron (a 5-HT<sub>3</sub> antagonist) for 60 min. Cross-sectional areas of organoids were compared. Mean  $\pm$  s.d., Kruskal–Wallis test followed by Dunn's multiple comparisons test.  $n = 40$  organoids. **f**, Intestinal organoids were incubated with 5  $\mu$ M A96 or 10  $\mu$ M RS 23597-190 for 12 h, and cross-sectional areas were compared. Mean  $\pm$  s.d., Kruskal–Wallis test followed by Dunn's multiple comparisons test.  $n$  (left to right) = 39, 40 and 40 organoids. **g, h**, Immunohistochemical labelling of 5-HT<sub>3</sub> receptors using a 5-HT<sub>3A</sub> nanobody conjugated to mCherry (VHH15–mCherry) in a nodose ganglion (**g**) and small intestine (**h**) isolated from *Htr3a*<sup>eGFP</sup> mice (*Htr3a* encodes 5-HT<sub>3</sub>). Each experiment was repeated three times. **i**, Distribution of the distances between the basolateral side of EC cells and the nearest nerve fibres. Mean  $\pm$  s.d. Scale bars 20  $\mu$ m (**a**), 50  $\mu$ m (**e, f, h**) or 100  $\mu$ m (**g**). The illustration in **g** was created using BioRender (<https://www.biorender.com>).

drugs on organoid proliferation (Extended Data Fig. 3d). On the basis of these findings, we conclude that TRPA1-dependent tonic serotonin release from crypt-residing EC cells activates 5-HT<sub>4</sub> receptors, which are predominantly localized in crypts, thereby stimulating ion secretion.

We next asked whether crypt and villus EC cells can target ionotropic 5-HT<sub>3</sub> receptors, which require micromolar serotonin for activation. It is known that both intrinsic and extrinsic sensory afferents express ionotropic 5-HT<sub>3</sub> receptors<sup>13,27,28</sup>. To further characterize the expression of 5-HT receptors in these sensory neurons, we first re-analysed a published scRNA-seq dataset<sup>29</sup>. The analysis showed that intrinsic primary afferent neurons predominantly express 5-HT<sub>3</sub> receptors, with minimal expression of other 5-HT receptor subtypes (Extended Data Fig. 4a). Next, we performed retrograde tracing from the small intestine mucosa and observed that the majority of labelled extrinsic mucosal afferents originate from nodose ganglia, with only sparse mucosal afferent innervation from dorsal root ganglia (Extended Data

Fig. 4b). Single-cell reverse transcription PCR (RT-PCR) analyses of these traced vagal mucosal neurons confirmed the expression of 5-HT<sub>3</sub> receptors and the absence of 5-HT<sub>4</sub> receptors (Extended Data Fig. 4c). To functionally validate these findings, we performed jejunal afferent recordings in the presence of a selective 5-HT<sub>4</sub> receptor antagonist. Consistent with the gene expression data, inhibition of 5-HT<sub>4</sub> receptors had no effect on basal nerve fibre activity (Extended Data Fig. 4d), a result that provides further support for the predominant role of 5-HT<sub>3</sub> receptors in mediating serotonergic signalling in mucosa-innervating sensory neurons. Collectively, these findings indicate that mucosa-innervating extrinsic sensory neurons require exposure to micromolar concentrations of serotonin for activation through 5-HT<sub>3</sub> receptors.

We then set out to determine the precise localization of 5-HT<sub>3</sub> receptors along nerve fibres. Specifically, we examined whether they are preferentially expressed near EC cells, concentrated at nerve terminals,

or broadly distributed along the nerve fibres. For this purpose, we used a modified 5-HT<sub>3A</sub>-specific nanobody (VHH15)<sup>30</sup> fused to mCherry, which specifically labelled heterologously expressed 5-HT<sub>3</sub> receptors or native receptors in nodose and dorsal root ganglia (Fig. 3g and Extended Data Fig. 5a,b). Labelled nerve fibres innervating the mucosa were seen in both the small and large intestine, which revealed uniform channel expression along the length of these afferents (Fig. 3h and Extended Data Fig. 5b).

Thus, EC cells in crypts or villi should be capable of activating mucosal afferents as long as the released transmitter reaches micromolar concentrations. To directly assess the propagation of EC-derived serotonin, we first established the distance between the basolateral side of EC cells and the closest nerve fibres (Fig. 3i and Extended Data Fig. 5c), which on average ( $5.5 \pm 4.5 \mu\text{m}$ ) was comparable to that between EC and biosensor cells used in the quantification experiments described above (Fig. 2). This finding indicated that most EC cells can present micromolar levels of serotonin to mucosal afferents when stimulated. Using *Insm1<sup>Cre</sup>;Rosa26<sup>(gGRAB<sub>5-HT3.0</sub>-iP2A-JRGECO1a)</sup>* sensor mice, which express gGRAB<sub>5-HT3.0</sub> in both EC cells and nerve fibres (Extended Data Fig. 5d), we could directly visualize the propagation of serotonin between EC cells and nerves. We observed that serotonin released from either crypt or villus EC cells readily reached and covered nearby nerve fibres (Extended Data Fig. 5e,f). In summary, our immunohistochemical and serotonin sensor analyses show that both crypt and villus EC cells are sufficiently close to 5-HT<sub>3</sub> receptors on mucosal sensory nerve fibres to transmit excitatory serotonergic signals to these afferents.

### Mucus degradation exposes TRPA1

We next investigated the physiological circumstances that might promote bolus serotonin release from crypt EC cells. As noted above, TRPA1 is an irritant-activated ion channel that responds to a wide range of electrophilic toxicants and inflammatory agents<sup>31</sup>. These include pungent agents from wasabi, garlic, onion and other members of the *Brassicaceae* and *Allium* plant family, which are associated with both potential health benefits and risks<sup>32,33</sup>. Also, environmental toxicants or metabolic by-products of certain chemotherapeutic drugs are strong electrophiles that induce severe inflammation in internal organs<sup>34</sup>. We were therefore curious to know whether such dietary electrophiles (AITC, allicin and cinnamaldehyde) or metabolites (acrolein and 2-pentenal) could activate crypt EC cells. In organoids from *Tac1<sup>Cre</sup>;Polr2a<sup>(GCaMP5g-IRES-tdTomato)</sup>* mice, each of these agents induced strong responses in EC cells that were blocked by the TRPA1 antagonist A96 (Fig. 4a and Extended Data Fig. 6a).

We next examined the effects of electrophiles in freshly prepared gut tissue, in which the crypt structure and its protective mucus layer are preserved. Using gGRAB<sub>5-HT3.0</sub> reporter mice, it was notable that only acrolein, a highly reactive electrophile, strongly stimulated crypt EC cells, whereas the other tested electrophiles were ineffective (Fig. 4b,c and Extended Data Fig. 6b). We reasoned that if the mucus layer acts as a barrier to irritant access, then its degradation should increase the susceptibility of crypt EC cells to weaker electrophiles. To test this hypothesis, we incubated gut tissue with StcE, a mucinase from pathogenic *Escherichia coli* O157 that digests MUC2, a primary component of intestinal mucus<sup>35,36</sup>. To determine whether StcE digestion enhances access to crypts, we exposed gut tissue to a fluorescently tagged electrophile, BODIPY-iodoacetamide (BODIPY-IA). In the presence of an intact mucus layer, BODIPY-IA infiltrated only the villus tips, even after 15 min of incubation (Fig. 4d). Notably, StcE treatment enabled BODIPY-IA to reach the crypts in as little as 3 min, a result that supported the idea that the mucus layer restricts electrophile access to the crypt region (Fig. 4d). Subsequently, we exposed StcE-treated intestinal tissue from gGRAB<sub>5-HT3.0</sub> mice to previously ineffective electrophiles and found that they readily activated crypt EC cells after mucus digestion (Fig. 4b,c and Extended Data Fig. 6c). Thus, we conclude that

under normal conditions, a protective mucus layer permits only potent and permeable electrophiles, such as acrolein, to access EC cells from the luminal side and to activate TRPA1. However, when this protective mucus barrier is compromised, then other electrophilic irritants, such as those from dietary sources, can gain access to crypt EC cells and stimulate serotonin release.

### TRPM2 senses oxidative stress in villi

Given that TRPA1 is preferentially expressed by crypt EC cells (Extended Data Fig. 2b,c), we wondered whether villus EC cells can also detect chemical irritants or other sentinels of tissue damage. Re-analysis of a published scRNA-seq dataset<sup>20</sup> revealed a gradient of *Trpm2* expression, with the highest transcript levels in villus EC cells and progressively lower expression towards crypts (Extended Data Fig. 2c). This finding was corroborated by our *in situ* hybridization analysis, which showed preferential expression of TRPM2 channels in villus EC cells (Extended Data Fig. 7a). TRPM2 is an excitatory ion channel activated by intracellular ADP-ribose, which is generated during oxidative stress<sup>37</sup>. Whole-cell patch-clamp recordings revealed ADP-ribose-activated inward currents in EC cells (Fig. 5a). These currents were attenuated by 2-aminoethoxydiphenyl borate (2-APB), which inhibits TRPM2, and reduced after replacement of extracellular Na<sup>+</sup> with NMDG<sup>+</sup>. Consistent with the expression pattern of TRPM2, we observed significantly larger ADP-ribose-activated currents in villus EC cells than in crypt EC cells (Fig. 5a).

We next asked whether oxidative stress activates villus EC cells. Using dissociated EC cells that express GCaMP5g, 200  $\mu\text{M}$  H<sub>2</sub>O<sub>2</sub> strongly activated villus EC cells. This activation was blocked by 2-APB, but not by A96, which demonstrated that this process depends on TRPM2 (Fig. 5b and Extended Data Fig. 7b). Furthermore, in a model of low-level intestinal inflammation induced by administration of an anti-CD3 antibody<sup>38</sup>, which increases epithelial cell apoptosis as indicated by the elevated number of cleaved caspase-3-positive cells (Extended Data Fig. 7c), we observed an increase in serotonin release in villi but not in crypts (Extended Data Fig. 7d,e). Notably, this increase in serotonin release was blocked by 2-APB, thereby confirming its dependence on TRPM2. These findings indicate that TRPM2 channels sense inflammatory stress within the villus epithelium.

### Villus ECs release both serotonin and ATP

Villus EC cells do not exhibit tonic serotonin release (Fig. 2a), and expression of 5-HT<sub>4</sub> receptors in villi is minimal (Fig. 3a,b). Given these findings, we proposed that villus EC cells might have distinct neurotransmitter release patterns and targets. Although it has been suggested that EC cells release ATP together with serotonin<sup>39</sup>, we tested this directly using a genetically encoded ATP sensor, gGRAB<sub>ATP1.0</sub> (ref. 40). EC cells within organoids or primary isolated EC cells were depolarized with high K<sup>+</sup> (assessed by GCaMP fluorescence) while we simultaneously monitored the gGRAB<sub>ATP1.0</sub> signal in neighbouring biosensor cells (Fig. 5c). We treated organoids with BMP4, a key regulator of crypt–villus axis differentiation<sup>18</sup>, which resulted in the loss of spontaneous EC cell activity (Extended Data Fig. 8a), a result indicative of successful crypt-to-villus transformation. ATP was only released from primary dissociated single villus cells or villus-differentiated organoids, but not from isolated primary crypts or organoids where crypt EC cells predominate (Fig. 5c,d and Extended Data Fig. 8b). Moreover, gGRAB<sub>ATP1.0</sub> signal was attenuated in the absence of extracellular Ca<sup>2+</sup>, which suggests that ATP is released together with serotonin through secretory vesicles (Fig. 5d).

To confirm whether released nucleotide contributes to sensory nerve fibre activation, we first investigated the sensitivity of mucosal afferents to ATP and serotonin. We traced and dissociated mucosa-innervating vagal neurons from the small intestine and performed single-cell Ca<sup>2+</sup> imaging<sup>41</sup> (Extended Data Fig. 8c). Notably, all traced mucosal vagal

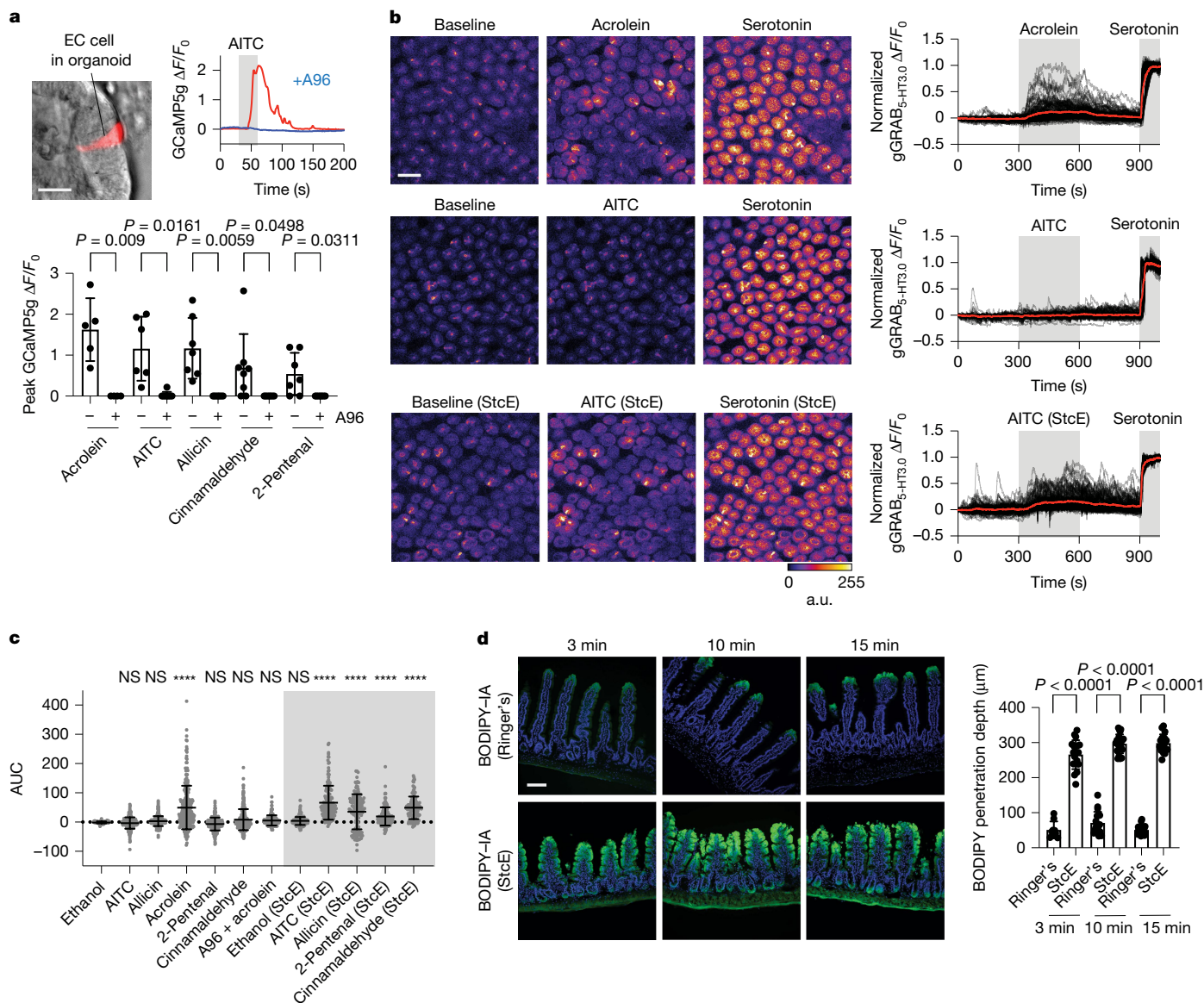


**Fig. 4 | TRPA1 is an electrophile sensor in the mucus-protected crypt EC cell.** **a**, Electrophiles activate EC cells within intestinal organoids derived from *Tacr<sup>Cre</sup>;Polr2a<sup>(GCaMP5g-ires-tdTomato)</sup>* mice. EC cells were stimulated by indicated electrophiles (100  $\mu$ M) with (blue) or without (red) 100  $\mu$ M A96. Mean  $\pm$  s.d., two-sided Welch's *t*-test. *n* = 7 cells. **b, c**, Electrophile activation of crypt EC cells ex vivo. Jejunal tissue was pretreated with StcE or saline and subsequently exposed to the indicated electrophiles (100  $\mu$ M) for 5 min. **b**, gGRAB<sub>5-HT3.0</sub> was fully activated with 20  $\mu$ M serotonin at the end of the recording, and signals were normalized to the fully activated value. **c**, Quantification of serotonin release in crypts. The area under the curve (AUC) was calculated during application of the agonist. Mean  $\pm$  s.d., Kruskal–Wallis test followed by Dunn's multiple comparisons test. Ethanol versus AITC, *P* > 0.9999 (not significant (NS)); ethanol versus allicin, *P* > 0.3169 (NS); ethanol versus acrolein, *P* < 0.0001;

ethanol versus 2-pentenal, *P* > 0.9999 (NS); ethanol versus cinnamaldehyde, *P* = 0.9514 (NS); ethanol versus acrolein + A96, *P* = 0.1469 (NS); ethanol versus ethanol (StcE), *P* = 0.2585 (NS). Ethanol (StcE) versus AITC (StcE), *P* < 0.0001; ethanol (StcE) versus allicin (StcE), *P* < 0.0001; ethanol (StcE) versus 2-pentenal (StcE), *P* < 0.0001; ethanol (StcE) versus cinnamaldehyde (StcE), *P* < 0.0001. *n* (left to right) = 93, 278, 263, 259, 233, 267, 176, 261, 161, 138, 161 and 120 crypts; *N* = 3 animals. \*\*\*\**P*  $\leq$  0.0001. **d**, Mucus limits the diffusion of electrophiles into the mucosal tissue. The ex vivo jejunal prep was exposed to 10 mM StcE or saline for 60 min. The tissue was then stained with 10  $\mu$ M BODIPY–IA for 3–15 min and the penetration depth was measured from the villus tips. Mean  $\pm$  s.d., two-sided Welch's *t*-test. *n* (left to right) = 9, 18, 18, 21, 20 and 21 villi per group. Scale bars, 20  $\mu$ m (**a**), 30  $\mu$ m (**b**) or 100  $\mu$ m (**d**).

neurons responded to ATP, and the majority also responded to the 5-HT<sub>3</sub> receptor-selective agonist mCPBG (Extended Data Fig. 8d,e). Consistent with these results, single-cell RT-PCR from these neurons revealed expression of genes that encode P2X and 5-HT<sub>3</sub> receptors (Extended Data Fig. 4c), which suggested that villus EC-derived ATP and serotonin collaborate to activate mucosal vagal afferents. Moreover, most of these neurons did not respond to AITC or H<sub>2</sub>O<sub>2</sub>, or express TRPA1 or TRPM2 channels. This result highlights the role of EC cells as primary specialized sensors for electrophiles and oxidative stress

in the small intestine that couple to mucosal afferents (Extended Data Figs. 4c and 8d,e).

To directly assess the contribution of EC-derived serotonin and ATP to mucosal afferent activation, we examined nerve fibre activity in *Tph1<sup>CreER</sup>;Rosa26<sup>(ls1-Chr2)</sup>* mice that express light-activated ion channels specifically in crypt and villus EC cells (Extended Data Fig. 8f,g). Using 'flat sheet' ex vivo afferent recording preparations, compound action potentials were measured from the jejunal mesenteric nerve bundle while stimulating EC cells with 470 nm light from the luminal side



significantly reduced light-induced spiking, with only 1.5% of fibres showing activation, but had minor effects on fibres with increased firing. The combination of both antagonists blocked almost all responses (Fig. 5f and Extended Data Fig. 8h). In summary, EC cells use both serotonin and ATP to signal to mucosa-innervating vagal afferents, with ATP input likely originating from villus EC cells.

Finally, we asked whether specific activation of crypt or villus EC cells leads to nerve fibre activity in a 5-HT<sub>3</sub>-dependent and/or P2X-dependent manner. We used *Scn10a*<sup>Cre</sup>;*Rosa26*<sup>(*lsl-ChR2*)</sup> mice, which express ChR2 in Na<sub>v</sub>1.8-positive sensory neurons, to optogenetically activate sensory nerve endings in the jejunum. This enabled us to test whether EC cell activation sensitizes nerve endings to light stimulation<sup>13</sup>, presumably through serotonin or ATP. Using ex vivo jejunal preparations from these mice, we applied either AITC (a weak electrophile) or acrolein (a strong electrophile) and recorded nerve fibre activity (Extended Data Fig. 9a). AITC application did not alter the baseline activity or light sensitivity of mucosal afferents (Extended Data Fig. 9b–d), whereas acrolein increased both (Extended Data Fig. 9e–g). This differential response aligned with our ex vivo serotonin sensor-imaging results, which demonstrated that crypt EC cells are responsive to strong but not weak electrophiles (Fig. 4b,c). Notably, the acrolein-induced effects were blocked by alosetron, but not PPADS, which indicated that crypt EC cells primarily use serotonin to activate mucosal afferents in response to strong electrophiles (Extended Data Fig. 9e–g).

To activate villus EC cells, we applied H<sub>2</sub>O<sub>2</sub>. This treatment increased both basal nerve activity and light sensitivity (Extended Data Fig. 10a–c). The effect was primarily PPADS-dependent, with alosetron showing only modest effects (Extended Data Fig. 10a–c), which suggested that villus EC cells predominantly use ATP, with a minor contribution from serotonin, to signal to mucosal afferents. In summary, our biosensor experiments and nerve fibre recordings demonstrate that crypt and villus EC cells respond to distinct stressors (electrophiles or oxidative stress) and favour different transmitters (serotonin or ATP) to communicate with mucosal afferents.

## Discussion

### Two modes of serotonin release

In this study, we developed and used biosensors to characterize the spatial and temporal dynamics of neurotransmitter signalling within the gut architecture with the goal of understanding the relevance of these parameters to homeostatic and protective functions. Previously, high-performance liquid chromatography and enzyme-linked immunosorbent assays were used to measure levels of gut serotonin<sup>42,43</sup>. However, these methods primarily measure serotonin extracted from entire tissue samples and typically provide single-timepoint measurements without spatial information. Voltage amperometry has also been used to detect gut serotonin<sup>44,45</sup>, but these measurements were primarily limited to luminal serotonin or concentrations on the villus surface. A more recent innovation, a tissue-like electrochemical biosensor, was designed to record serotonin levels in the intact intestine, but this method also predominantly measures luminal serotonin<sup>46</sup>. By comparison, our approach provides enhanced spatial, temporal and quantitative analyses that improve our understanding of how specific stimuli trigger transmitter release from sensory cells within a complex anatomical structure, in this case, the crypt-villus architecture with an intact mucus layer. By directing the expression of serotonin sensors to all intestinal epithelial cells, we were able to visualize the extent of diffusion of EC-derived serotonin within the epithelial layer after activation. Another noteworthy feature of gGRAB<sub>5-HT<sub>3</sub></sub> is its independence from arrestin-mediated desensitization<sup>23</sup>, which enables extended (>30 min) imaging and normalization of signals after the addition of a saturating agonist concentration, thereby increasing the quantitative robustness of the method.

Using these tools, we demonstrated that EC cells within the crypt release serotonin in two ways: low-level tonic and high-level-induced modes. An important question that remains to be answered is the underlying mechanism of TRPA1-dependent tonic release. Our patch-clamp experiments showed that basal TRPA1 activity occurs in cultured EC cells and that single-channel events sufficiently depolarized the membrane to activate Na<sub>v</sub> channels and induce action potentials. Thus, tonic transmitter release is probably a cell-autonomous process driven by low-level TRPA1 activity that is either spontaneous or induced by tonic low-level production of cellular electrophiles. TRPA1 is also a 'receptor operated' channel that can be activated downstream of signalling pathways that increase cytosolic calcium, thereby representing another potential regulatory mechanism<sup>47</sup>. The identification of factors or conditions that support tonic channel activation may provide insights into endogenous or metabolic processes that regulate basal EC cell excitability. Nevertheless, our findings indicated that crypt EC cells constitutively modulate ion secretion through 5-HT<sub>4</sub> receptor-expressing cells located within the crypt. Consistent with this result, it has been shown that a 5-HT<sub>4</sub> antagonist decreases basal ion secretion in the small intestine<sup>15</sup>. Therefore, crypt EC cells may fine-tune ion secretion in response to changes in luminal or endogenous electrophiles that access crypts. Notably, this low level of tonically released serotonin did not activate 5-HT<sub>3</sub> receptors on sensory neurons, which suggests that crypt EC cells control gut secretion without conveying signals to intrinsic or extrinsic sensory networks, except perhaps in extreme pathological circumstances that degrade the protective mucus layer (see below).

It has been proposed that enteroendocrine L cells communicate with sensory neurons through synapse-like contacts<sup>48</sup>, an idea that we subsequently suggested might also apply to interactions between EC cells and primary afferents<sup>4</sup>. Although a subset of EC cells and nerve fibres are closely juxtaposed, our current analysis indicated that the majority are too distant to establish bona fide synapses and probably communicate in a paracrine manner. Consistent with our measurements, recent studies have demonstrated that most colonic and small intestinal EC cells are similarly too distant to form synapses with spinal and vagal afferents, respectively<sup>49,50</sup>. These analyses of small intestinal EC cells and vagal afferents measured an average distance of 25.7 μm, which is greater than what we report here. This discrepancy probably reflects the fact that our analysis encompassed all nerve fibres, including intrinsic primary afferents and extrinsic afferent neurons, whereas their tracing studies labelled only a subset of vagal afferents. Nevertheless, our findings indicated that despite these distances, communication still occurs, as released serotonin diffused towards the closest nerve fibre, which uniformly express 5-HT<sub>3</sub> receptors along their length. Our observations also suggest that when multiple EC cells within the same villus or adjacent crypts are simultaneously activated, they collaborate to stimulate the same nerve fibres. Thus, we propose that sparsely distributed EC cells integrate the information within the local environment in a parallel processing manner, converging their signals to produce a single output to the nervous system to transmit signals within or outside the gut.

### Mucus is a barrier for irritants

The mucus layer is thickest over crypts, providing protection for stem cells that regenerate the intestinal epithelium. It therefore makes sense that TRPA1 channels are located preferentially in this protected zone, where they can serve as sentinels for highly reactive irritants such as acrolein, the ingestion of which leads to frequent vomiting in dogs<sup>51</sup>. Acrolein, an environmental toxicant, is found in fried foods and alcoholic beverages and produced by catabolism of cyclophosphamide and related chemotherapeutic agents<sup>52</sup>. Acrolein may also be produced by microbial metabolism of glycerol in the gut, thereby representing another pathological scenario in which EC cell activation initiates protective nocifensive signals<sup>52</sup>.

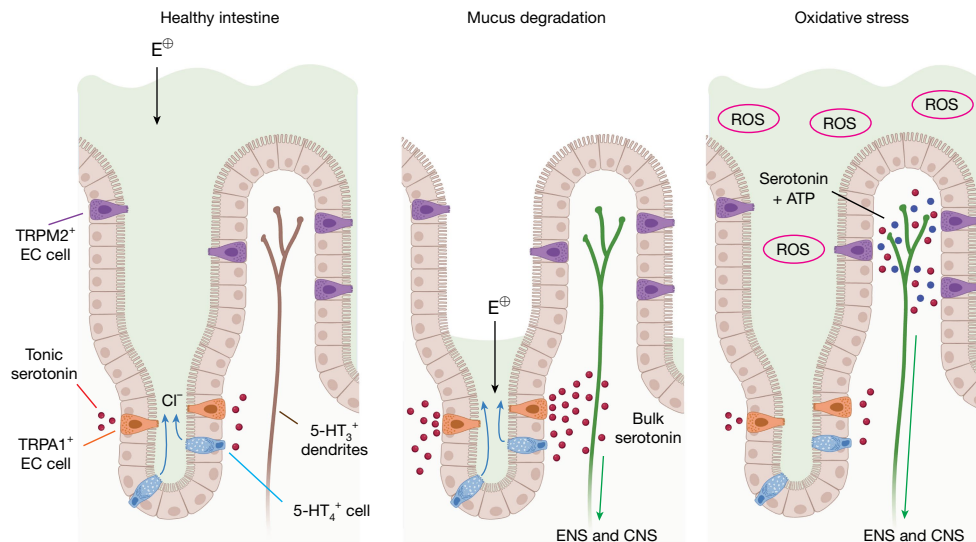


**Fig. 6 | Compartmentalized EC cell signalling in intestinal stress responses.**

In the healthy intestine, mucus shields the epithelium from luminal electrophiles ( $E^+$ ), whereas the tonic, TRPA1-dependent activity of EC cells regulates ion secretion from crypts. After damage to the mucus layer, luminal electrophiles further activate crypt EC cells, stimulating a bolus of serotonin release that activates the mucosal nerve fibres to relay signals to the enteric

and central nervous systems (ENS and CNS, respectively). Villus EC cells are silent in the healthy intestine. These cells detect increased ROS through the activation of TRPM2 and signal to the mucosal nerve fibres through purinergic and serotonergic neurotransmission. The illustration was created using BioRender (<https://www.biorender.com>).

Weaker electrophiles found in foods such as mustard, garlic and onions do not usually induce an extreme nocifensive reflex, consistent with our finding that they do not penetrate the mucus layer to stimulate TRPA1 channels on crypt EC cells. In pathological states such as colitis or bacterial infection, where the mucus layer is compromised<sup>53</sup>, these dietary electrophiles could potentially breach this protective barrier to activate crypt EC cells and promote nausea. This is consistent with observations that patients with inflammatory bowel disease often avoid spicy foods, including mustard and garlic, thereby suggesting that these individuals have heightened exposure of their crypt EC cells to luminal contents<sup>54</sup>. Also, differential sensitivity to endogenous or exogenous electrophiles will probably reflect individual variations in the status of the protective mucosal barrier, which is influenced by factors such as microbiota and dietary habits<sup>55</sup>. Notably, crypt EC cells tonically stimulate ion secretion, which presumably regulates the hydration status of intestinal contents near crypts, regardless of the condition of the mucus layer. This tonic regulation may also be tuned according to the permeability of electrophiles towards the crypts, but as noted above, nerve fibres should only be recruited when electrophiles penetrate the barrier in sufficient quantities to activate TRPA1 channels.

### Detecting stress signals in villi

TRPA1 is activated by reactive oxygen species (ROS) such as  $H_2O_2$  and 4-hydroxynonenal, which makes this receptor a key physiological sensor of oxidative stress and cellular redox state<sup>56</sup>. TRPM2 is also activated by  $H_2O_2$ , and our results suggest that these two TRP channel subtypes function as irritant and ROS sensors in crypts and villi, respectively (Fig. 6). Unlike TRPA1 receptors in crypts, TRPM2 channels in villi are not as well shielded by a thick mucus layer and may therefore serve as ‘first responders’ to oxidative stress. Moreover, the ability of activated villus EC cells to simultaneously release serotonin and ATP augments their capacity to strongly stimulate mucosa-innervating vagal neurons, most or all of which are activated by both transmitters.

Although EC cells have long been recognized primarily as serotonin-releasing cells, our data reveal a role for ATP as a transmitter, with a notable segregation to a topologically specific population of EC cells in villi. How this specification is established remains an interesting question for future studies. Regardless, these findings necessitate

a re-evaluation of how purinergic receptors contribute to EC cell-mediated vagal and intrinsic primary afferent activation, and its subsequent impact on physiological responses, including nausea sensations and changes in gut motility. Although ATP is widely appreciated as an activator of primary afferents<sup>57</sup>, purinergic receptors are also expressed by other cell types in the gut, such as enteric glia ( $P2X_7$ ), enterocytes ( $P2X_7$ ) and secretomotor neurons ( $P2Y_1$ )<sup>58</sup>; therefore, it is possible that villus EC cells target these receptors to trigger additional stress responses.

ROS are produced in pathological situations such as inflammatory bowel disease and chronic granulomatous disease<sup>59</sup>. Furthermore, chemotherapeutic drugs can rapidly generate ROS during the initial treatment stages, causing damage to the intestinal mucosa<sup>59</sup>. Our findings indicate that ROS produced in these individuals may activate TRPM2 in villus EC cells, triggering GI pain and nausea. With the loss of the protective mucus layer, TRPA1 channels in the crypt may then be recruited, thereby further contributing to nociceptive and neurogenic inflammatory responses. Several TRPA1 antagonists have undergone clinical trials for managing inflammatory pain or airway hypersensitivity<sup>60</sup>. Our work now highlights their potential use for treating GI symptoms associated with the overproduction of reactive irritants (of microbial or inflammatory origin) or reduction of the protective mucosal barrier. The same may pertain to potent and selective TRPM2 inhibitors, which are currently lacking.

### Online content

Any methods, additional references, Nature Portfolio reporting summaries, source data, extended data, supplementary information, acknowledgements, peer review information; details of author contributions and competing interests; and statements of data and code availability are available at <https://doi.org/10.1038/s41586-024-08581-9>.

- Gershon, M. D. 5-Hydroxytryptamine (serotonin) in the gastrointestinal tract. *Curr. Opin. Endocrinol. Diabetes Obes.* **20**, 14–21 (2013).
- Mawe, G. M. & Hoffman, J. M. Serotonin signalling in the gut functions, dysfunctions and therapeutic targets. *Nat. Rev. Gastroenterol. Hepatol.* **10**, 473–486 (2013).
- Nozawa, K. et al. TRPA1 regulates gastrointestinal motility through serotonin release from enterochromaffin cells. *Proc. Natl Acad. Sci. USA* **106**, 3408–3413 (2009).

4. Bellono, N. W. et al. Enterochromaffin cells are gut chemosensors that couple to sensory neural pathways. *Cell* **170**, 185–198 (2017).
5. Chen, Z. et al. Interleukin-33 promotes serotonin release from enterochromaffin cells for intestinal homeostasis. *Immunity* **54**, 151–163 (2021).
6. Lund, M. L. et al. Enterochromaffin 5-HT cells—a major target for GLP-1 and gut microbial metabolites. *Mol. Metab.* **11**, 70–83 (2018).
7. Gribble, F. M. & Reimann, F. Enteroendocrine cells: chemosensors in the intestinal epithelium. *Annu. Rev. Physiol.* **78**, 277–299 (2016).
8. Erspamer, V. & Asero, B. Identification of enteramine, the specific hormone of the enterochromaffin cell system, as 5-hydroxytryptamine. *Nature* **169**, 800–801 (1952).
9. Strege, P. R. et al. Sodium channel Na<sub>v</sub>1.3 is important for enterochromaffin cell excitability and serotonin release. *Sci. Rep.* **7**, 15650 (2017).
10. Mawe, G. M., Hurd, M., Hennig, G. W. & Lavoie, B. Epithelial 5-HT<sub>4</sub> receptors as a target for treating constipation and intestinal inflammation. *Adv. Exp. Med. Biol.* **1383**, 329–334 (2022).
11. Thompson, A. J. & Lummiss, S. C. 5-HT<sub>4</sub> receptors. *Curr. Pharm. Des.* **12**, 3615–3630 (2006).
12. Xie, Z. et al. The gut-to-brain axis for toxin-induced defensive responses. *Cell* **185**, 4298–4316 (2022).
13. Bayrer, J. R. et al. Gut enterochromaffin cells drive visceral pain and anxiety. *Nature* **616**, 137–142 (2023).
14. Bockaert, J., Claeysen, S., Compan, V. & Dumuis, A. 5-HT<sub>4</sub> receptors. *Curr. Drug Targets CNS Neurol. Disord.* **3**, 39–51 (2004).
15. Tough, I. R., Lund, M. L., Patel, B. A., Schwartz, T. W. & Cox, H. M. Paracrine relationship between incretin hormones and endogenous 5-hydroxytryptamine in the small and large intestine. *Neurogastroenterol. Motil.* **35**, e14589 (2023).
16. Barrett, K. E. & Keely, S. J. Chloride secretion by the intestinal epithelium: molecular basis and regulatory aspects. *Annu. Rev. Physiol.* **62**, 535–572 (2000).
17. Peterson, L. W. & Artis, D. Intestinal epithelial cells: regulators of barrier function and immune homeostasis. *Nat. Rev. Immunol.* **14**, 141–153 (2014).
18. Beumer, V. B. et al. Enteroendocrine cells switch hormone expression along the crypt-to-villus BMP signalling gradient. *Nat. Cell Biol.* **20**, 909–916 (2018).
19. Song, Y. et al. Stratification of enterochromaffin cells by single-cell expression analysis. Preprint at *bioRxiv* <https://doi.org/10.1101/2023.08.24.554649> (2023).
20. Hayashi, M. et al. Enteroendocrine cell lineages that differentially control feeding and gut motility. *eLife* **12**, e78512 (2023).
21. Bertrand, P. P. & Bertrand, R. L. Serotonin release and uptake in the gastrointestinal tract. *Auton. Neurosci.* **153**, 47–57 (2010).
22. Wan, J. et al. A genetically encoded sensor for measuring serotonin dynamics. *Nat. Neurosci.* **24**, 746–752 (2021).
23. Deng, F. et al. Improved green and red GRAB sensors for monitoring spatiotemporal serotonin release in vivo. *Nat. Methods* **21**, 692–702 (2024).
24. Madison, B. B. et al. *Cis* elements of the *villin* gene control expression in restricted domains of the vertical (crypt) and horizontal (duodenum, cecum) axes of the intestine. *J. Biol. Chem.* **277**, 33275–33283 (2002).
25. McCorvy, J. D. et al. Structural determinants of 5-HT<sub>2B</sub> receptor activation and biased agonism. *Nat. Struct. Mol. Biol.* **25**, 787–796 (2018).
26. Boj, S. F. et al. Forskolin-induced swelling in intestinal organoids: an in vitro assay for assessing drug response in cystic fibrosis patients. *J. Vis. Exp.* <https://doi.org/10.3791/55159-v> (2017).
27. Bai, L. et al. Genetic identification of vagal sensory neurons that control feeding. *Cell* **179**, 1129–1143 (2019).
28. Fung, C. et al. Luminal nutrients activate distinct patterns in submucosal and myenteric neurons in the mouse small intestine. Preprint at *bioRxiv* <https://doi.org/10.1101/2021.01.19.427232> (2021).
29. Morarach, K. et al. Diversification of molecularly defined myenteric neuron classes revealed by single-cell RNA sequencing. *Nat. Neurosci.* **24**, 34–46 (2021).
30. Hassaine, G. et al. X-ray structure of the mouse serotonin 5-HT<sub>3</sub> receptor. *Nature* **512**, 276–281 (2014).
31. Bautista, D. M. et al. TRPA1 mediates the inflammatory actions of environmental irritants and proalgesic agents. *Cell* **124**, 1269–1282 (2006).
32. Nilius, B. & Appendino, G. Spices: the savory and beneficial science of pungency. *Rev. Physiol. Biochem. Pharmacol.* **164**, 1–76 (2013).
33. LoPachin, R. M., Geohagen, B. C. & Nordstroem, L. U. Mechanisms of soft and hard electrophile toxicities. *Toxicology* **418**, 62–69 (2019).
34. Achanta, S. & Jordt, S. E. TRPA1: acrolein meets its target. *Toxicol. Appl. Pharmacol.* **324**, 45–50 (2017).
35. Hews, C. L. et al. The StcE metalloprotease of enterohaemorrhagic *Escherichia coli* reduces the inner mucus layer and promotes adherence to human colonic epithelium ex vivo. *Cell. Microbiol.* **19**, e12717 (2017).
36. Malaker, S. A. et al. The mucin-selective protease StcE enables molecular and functional analysis of human cancer-associated mucins. *Proc. Natl Acad. Sci. USA* **116**, 7278–7287 (2019).
37. Perraud, A. L. et al. ADP-ribose gating of the calcium-permeable LTRPC2 channel revealed by Nudix motif homology. *Nature* **411**, 595–599 (2001).
38. Miura, N. et al. Anti-CD3 induces bi-phasic apoptosis in murine intestinal epithelial cells: possible involvement of the Fas/Fas ligand system in different T cell compartments. *Int. Immunol.* **17**, 513–522 (2005).
39. Linan-Rico, A. et al. Purinergic autocrine regulation of mechanosensitivity and serotonin release in a human EC model: ATP-gated P2X<sub>3</sub> channels in EC are downregulated in ulcerative colitis. *Inflamm. Bowel Dis.* **19**, 2366–2379 (2013).
40. Wu, Z. et al. A sensitive GRAB sensor for detecting extracellular ATP in vitro and in vivo. *Neuron* **110**, 770–782 (2022).
41. Harrington, A. M. et al. Colonic afferent input and dorsal horn neuron activation differs between the thoracolumbar and lumbosacral spinal cord. *Am. J. Physiol. Gastrointest. Liver Physiol.* **317**, G285–G303 (2019).
42. Kumar, A. et al. The serotonin neurotransmitter modulates virulence of enteric pathogens. *Cell Host Microbe* **28**, 41–53 (2020).
43. Reigstad, C. S. et al. Gut microbes promote colonic serotonin production through an effect of short-chain fatty acids on enterochromaffin cells. *FASEB J.* **29**, 1395–1403 (2015).
44. Bertrand, P. P., Bertrand, R. L., Camello, P. J. & Pozo, M. J. Simultaneous measurement of serotonin and melatonin from the intestine of old mice: the effects of daily melatonin supplementation. *J. Pineal Res.* **49**, 23–34 (2010).
45. Patel, B. A., Bian, X., Quaiserová-Mocko, V., Galligan, J. J. & Swain, G. M. In vitro continuous amperometric monitoring of 5-hydroxytryptamine release from enterochromaffin cells of the guinea pig ileum. *Analyst* **132**, 41–47 (2007).
46. Li, J. et al. A tissue-like neurotransmitter sensor for the brain and gut. *Nature* **606**, 94–101 (2022).
47. Zhao, J., Lin King, J. V., Paulsen, C. E., Cheng, Y. & Julius, D. Irritant-evoked activation and calcium modulation of the TRPA1 receptor. *Nature* **585**, 141–145 (2020).
48. Kaelberer, M. M. et al. A gut–brain neural circuit for nutrient sensory transduction. *Science* **361**, eaat5236 (2018).
49. Dodds, K. N. et al. The gut–brain axis: spatial relationship between spinal afferent nerves and 5-HT-containing enterochromaffin cells in mucosa of mouse colon. *Am. J. Physiol. Gastrointest. Liver Physiol.* **322**, G523–G533 (2022).
50. Spencer, N. J., Kyloh, M. A., Travis, L. & Hibberd, T. J. Identification of vagal afferent nerve endings in the mouse colon and their spatial relationship with enterochromaffin cells. *Cell Tissue Res.* **396**, 313–327 (2024).
51. Parent, R. A., Caravello, H. E., Balmer, M. F., Shellenberger, T. E. & Long, J. E. One-year toxicity of orally administered acrolein to the beagle dog. *J. Appl. Toxicol.* **12**, 311–316 (1992).
52. Zhang, J., Sturla, S., Lacroix, C. & Schwab, C. Gut microbial glycerol metabolism as an endogenous acrolein source. *mBio* **9**, e01947-17 (2018).
53. Tarabova, L., Makova, Z., Piesova, E., Szaboova, R. & Faixova, Z. Intestinal mucus layer and mucins (a review). *Folia Vet.* **60**, 21–25 (2016).
54. Limdi, J. K. Dietary practices and inflammatory bowel disease. *Indian J. Gastroenterol.* **37**, 284–292 (2018).
55. Paone, P. & Cani, P. D. Mucus barrier, mucins and gut microbiota: the expected slimy partners? *Gut* **69**, 2232–2243 (2020).
56. Andersson, D. A., Gentry, C., Moss, S. & Bevan, S. Transient receptor potential A1 is a sensory receptor for multiple products of oxidative stress. *J. Neurosci.* **28**, 2485–2494 (2008).
57. North, R. A. P2X<sub>3</sub> receptors and peripheral pain mechanisms. *J. Physiol.* **554**, 301–308 (2004).
58. Burnstock, G. P2X receptors in the gut. *WIREs Membr. Transp. Signal.* **1**, 269–279 (2011).
59. Aviello, G. & Knaus, U. G. ROS in gastrointestinal inflammation: rescue or sabotage? *Br. J. Pharmacol.* **174**, 1704–1718 (2017).
60. Koivisto, A. P., Belvisi, M. G., Gaudet, R. & Szallasi, A. Advances in TRP channel drug discovery: from target validation to clinical studies. *Nat. Rev. Drug Discov.* **21**, 41–59 (2022).

**Publisher's note** Springer Nature remains neutral with regard to jurisdictional claims in published maps and institutional affiliations.

Springer Nature or its licensor (e.g. a society or other partner) holds exclusive rights to this article under a publishing agreement with the author(s) or other rightsholder(s); author self-archiving of the accepted manuscript version of this article is solely governed by the terms of such publishing agreement and applicable law.

© The Author(s), under exclusive licence to Springer Nature Limited 2025

## Methods

### Mice

All experimental procedures were conducted in accordance with guidelines approved by the Institutional Animal Care Committees at UCSF, the SAHMRI Animal Ethics Committee and Peking University, and aligned with the NIH's Guide for the Care and Use of Laboratory Animals. Mice of both sexes aged 8–16 weeks old were used and given ad libitum access to standard laboratory chow and sterile water. The mice were housed in a controlled environment under a 12-h light–dark cycle. For serotonin sensor imaging, *Vil1<sup>Cre</sup>* mice (Jackson Laboratory, 021504) and *Insm1-GFP<sup>Cre</sup>* mice (gift from C. Harwell; MMRRC ID: 36986) were crossed to the gGRAB<sub>5-HT<sub>3.0</sub></sub>-P2A-jRGECO1a reporter line. For nerve fibre recordings, *Tph1<sup>CreER</sup>* mice<sup>61</sup> (gift from J. L. Merchant, University of Arizona College of Medicine) or *Scn10a<sup>Cre</sup>* (gift from W. Imlach, Monash University, Australia; Jackson Laboratory, 036564) were crossed to the Chr2 (Ai32D) reporter line (Jackson Laboratory, 012569). GCaMP imaging in organoids used *Tac1<sup>Cre</sup>* mice (Jackson Laboratory, 021877) crossed with *Polr2a<sup>(GCaMP5g-IRES-tdTomato)</sup>* reporter mice (gift from L. Jan, UCSF; Jackson Laboratory, 024477). Excitatory DREADD hM3Dq receptors were expressed in EC cells using *Tac1<sup>Cre</sup>;ePet1-Flp*;RC::FL-hM3Dq mice. *Htr3a<sup>eGFP</sup>* mice (MMRRC ID: 000273) were used to visualize 5-HT<sub>3</sub>-expressing nerve fibres. *Pirt1<sup>Cre</sup>* mice (gift from X. Dong, Johns Hopkins Medicine) were crossed with Ai14 tdTomato reporter mice (Jackson Laboratory, 007914) for mucosal nerve fibre visualization.

### Epithelial cell isolation and organoid culture

Adult male *Tac1<sup>Cre</sup>;Polr2a<sup>(GCaMP5g-IRES-tdTomato)</sup>* mice were used to generate intestinal organoids as previously reported<sup>62</sup>. The upper jejunum was specifically used to avoid ectopic *Tac1<sup>Cre</sup>* expression in the lower intestine. Organoids were maintained and passaged every 6 days in organoid growth medium (advanced Dulbecco's modified Eagle's medium–F12 supplemented with penicillin–streptomycin, 10 mM HEPES, Glutamax, B27 (Thermo Fisher Scientific), 1 mM *N*-acetylcysteine (Sigma), 50 ng ml<sup>-1</sup> mouse recombinant epidermal growth factor (Thermo Fisher Scientific), R-spondin 1 (10% final volume) and 100 ng ml<sup>-1</sup> murine Noggin (Peprotech)). For villus organoid differentiation, day 4 organoids were treated with 5 μM IWP2 (Stemgent), 10 μM DAPT (Sigma), 1 μM PDO325901 (Sigma) and 20 ng ml<sup>-1</sup> BMP4 (Peprotech) for 4 days.

### Cell lines

HEK293FT cells (Thermo Fisher Scientific) were maintained in DMEM, 10% FCS and 1% penicillin–streptomycin. The R-spondin 1-expressing HEK293T cells (Sigma) were maintained in DMEM, 20% FCS, 1% penicillin–streptomycin and 125 μg ml<sup>-1</sup> zeocin (Thermo Fisher Scientific) at 37 °C, 5% CO<sub>2</sub>. Zeocin was removed after the production of R-spondin 1-conditioned medium. HEK cells were transfected using Lipofectamine 3000 (Thermo Fisher Scientific) according to the manufacturer's protocol. For biosensor experiments, 200 ng pDisplay-gGRAB<sub>5-HT<sub>2m</sub></sub>-IRES-mCherryCAAX (Addgene, 208710), 200 ng pcDNA3-5-HT<sub>2A</sub>-P2A-GCaMP8m or 200 ng pDisplay-gGRAB<sub>ATP1.0</sub>-IRES-mCherryCAAX (Addgene, 167582) was transfected into HEK293T cells in 24-well plates. For 5-HT<sub>3</sub> biosensor experiments, 200 ng pcDNA3-5-HT<sub>3A</sub> and 20 ng pcDNA3-mApple were co-transfected into HEK293T cells in 24-well plates.

### Generation of gGRAB<sub>5-HT<sub>3.0</sub></sub>-P2A-jRGECO1a reporter mice

The gGRAB<sub>5-HT<sub>3.0</sub></sub>-P2A-jRGECO1a reporter mouse line was generated with the help of Biocytogen Pharmaceuticals. In detail, the CAG-*loxP*-STOP-*loxP*-gGRAB<sub>5-HT<sub>3.0</sub></sub>-P2A-jRGECO1a-WPRE-bGH sequence was inserted to the *Rosa26* locus of mouse embryonic stem cells using CRISPR–Cas9-mediated homology-directed repair. Successful targeting was confirmed by PCR. The genetically modified embryonic stem cells were injected into eight-cell-stage embryos to generate chimeric mice. The chimeric mice were then mated with wild-type mice to obtain

germline transmission of the targeted allele. The resulting transgenic mouse line stably expresses both gGRAB<sub>5-HT<sub>3.0</sub></sub> and jRGECO1a under the CAG promoter at the *Rosa26* locus after excision of the floxed stop cassette by Cre recombinase.

### Anti-CD3 antibody-induced inflammation model

Mice received a single intraperitoneal injection of 30 μg anti-CD3 antibody (Thermo Fisher Scientific) diluted to 200 μl with physiological saline. Mice were killed for tissue collection after 12 h.

### Ex vivo serotonin sensor imaging

Approximately 1 cm pieces of jejunum were isolated from 8–16-week old *Vil1<sup>Cre</sup>;Rosa26<sup>(gGRAB<sub>5-HT<sub>3.0</sub>-iP2A-jRGECO1a)</sub></sup>* mice or *Insm1-GFP<sup>Cre</sup>;Rosa26<sup>(gGRAB<sub>5-HT<sub>3.0</sub>-iP2A-jRGECO1a)</sub></sup>* mice. The isolated tissue was then immediately dissected open along the mesentery, pinned down to a Sylgard-coated recording chamber and imaged from the smooth muscle side to observe crypts and from the luminal side to observe villi. Imaging was performed with a Leica SP8 confocal microscope with a HC APO L ×20/1,00 W objective and LAS X software (Leica Microsystems, v.3.5.5.19976). The tissue was bath-perfused with bubbled room-temperature Krebs buffer (118 mM NaCl, 4.7 mM KCl, 1 mM MgCl<sub>2</sub>, 2 mM CaCl<sub>2</sub>, 1.2 mM KH<sub>2</sub>PO<sub>4</sub>, 25 mM NaHCO<sub>3</sub> and 10 mM D-glucose) at a rate of about 1 ml min<sup>-1</sup>. All pharmacological reagents were diluted in Krebs buffer and bath-perfused with simultaneous manual application. For recordings of StcE-digested tissue, 50 μM StcE was added to Krebs buffer. At the end of each recording, gGRAB<sub>5-HT<sub>3.0</sub></sub> was fully activated by bath-applied 20 μM serotonin. Acquired images were analysed using Fiji software (v.2.14, NIH). The ROIs were drawn around individual crypts or villi and  $\Delta F/F_0$  were calculated and normalized to serotonin-activated maximum signals. The AUC was calculated as the normalized gGRAB<sub>5-HT<sub>3.0</sub></sub>  $\Delta F/F_0$  for the duration of 5 min during baseline or drug application. When measuring baseline serotonin levels in villi, 20 μM RS 23597-190 was added at the end of recordings to fully quench the sensor.

### Serotonin sensor imaging with isolated villi and crypts

Pieces of jejunum were isolated from 8–16-week-old *Vil1<sup>Cre</sup>;Rosa26<sup>(gGRAB<sub>5-HT<sub>3.0</sub>-iP2A-jRGECO1a)</sub></sup>* mice. The isolated tissue was then dissected open along the mesentery. For recordings from isolated villi, villi were scraped off using glass coverslips and resuspended in a 50% Matrigel–Krebs buffer mixture. Matrigel domes (about 5 μl) were then formed on glass coverslips for imaging. The villi exposed to the surface of the Matrigel domes were identified using a microscope and used for imaging. For recordings from isolated crypts, after removal of the villi, the tissue was incubated in 10 ml cold Dulbecco's PBS (DPBS) with 30 mM EDTA for 20 min, followed by vigorous shaking for 30–60 s. Isolated crypts were filtered through 70 μm strainers and plated onto CellTak (Corning)-coated coverslips. Serotonin sensor imaging was performed with an upright microscope equipped with a Grasshopper 3 (FLIR) camera run using Micro-Manager software (v.2.0) and a Lambda LS light source (Sutter). Villi and crypts were maintained under a constant laminar flow of Ringer's solution applied by a pressure-driven microperfusion system (SmartSquirt, Automate Scientific). All pharmacological reagents were delivered by local perfusion. Acquired images were analysed using Fiji software (NIH). ROIs were drawn around individual EC cells and the  $\Delta F/F_0$  values were calculated.

### Expression and purification of StcE

The pET28b-StcE-Δ35-NHis plasmid (gift from C. Bertozzi, Stanford University) was transformed into *E. coli* BL21(DE3) cells. Transformed *E. coli* cells were cultured in LB medium containing 50 μg l<sup>-1</sup> kanamycin at 37 °C for 4 h. Isopropyl-thio-β-D-galactopyranoside was added to a final concentration of 0.3 mM to induce protein expression. Following an additional incubation at 20 °C for 12 h, cells were collected by centrifugation and resuspended in purification buffer (500 mM NaCl and

20 mM HEPES-Na (pH 7.5)). Cell extracts were obtained by sonication followed by centrifugation at 36,000g for 30 min. The supernatant was incubated with 2 ml Ni-NTA (Qiagen) for 1 h at 4 °C with gentle mixing. The resin was washed in batch with 5 column volumes of purification buffer, then loaded onto a column and further washed with 5 column volumes of purification buffer and 20 mM imidazole, and with 10 column volumes of purification buffer and 30 mM imidazole. The column was then eluted with purification buffer and 250 mM imidazole. To remove imidazole, the eluted protein was concentrated to 30 mM and then dialysed against purification buffer overnight. Purified proteins were stored at 4 °C.

#### Mucus digestion with StcE

Purified StcE (30 mM) was diluted to 10 mM with double-distilled H<sub>2</sub>O, and 1 M HEPES-Na (pH 7.5) solution was added to a final concentration of 20 mM. This dilution was performed immediately before the experiment to avoid precipitation of StcE. The isolated jejunum (about 1 cm) was incubated in 10 ml of 10 mM StcE for 60 min at room temperature with gentle shaking. The StcE solution was exchanged after 30 min. Digested tissue samples were immediately mounted on a recording chamber for gGRAB<sub>5-HT3.0</sub> imaging.

#### BODIPY-IA staining

A 10 mM StcE solution was prepared as described above. Sections of the jejunum (about 1 cm) were transferred to 10 ml of a solution of 166 mM NaCl and 20 mM HEPES-Na (pH 7.5) with or without 10 mM StcE and incubated for 30 min at room temperature with gentle shaking. Digested tissue samples were immediately transferred to 10 μM BODIPY-FL-IA (Thermo Fisher Scientific) in DPBS and incubated for 3–15 min at room temperature with gentle shaking. Stained tissues were briefly rinsed with DPBS and fixed with 4% paraformaldehyde (PFA) for 3 h at 4 °C. Fixed tissue samples were dehydrated in 30% sucrose overnight at 4 °C. The tissue samples were embedded in Tissue-Tek OCT compound (Sakura Finetek) and subsequently sectioned at a thickness of 10 μm on a Leica CM3050 S cryostat. The nuclei were stained with 4,6-diamidino-2-phenylindole (DAPI, 0.5 μg ml<sup>-1</sup>, Thermo Fisher Scientific) and sections were mounted with ProLong Diamond antifade mountant (Thermo Fisher Scientific). Confocal images were captured on an inverted Nikon Ti microscope run using Micro Manager 2.0 Gamma<sup>63</sup>, equipped with a Zyla 4.2 CMOS camera (Andor), a piezo xyz stage (ASI), a CSU-W1 spinning disk with Borealis upgrade (Yokogawa/Andor), Spectra-X (Lumencor) and an ILE 4 line laser launch (405/488/561/640 nm; Andor). Images were taken using a Plan Apo λ ×20/0.75 using lasers 405, 488 and 561 nm and emission filters 447/60, 525/50 and 607/36, for DAPI, GFP and RFP, respectively. Maximum-intensity projections were generated using Fiji (v.2.14).

#### Expression and purification of the 5-HT<sub>3</sub> nanobody

The 5-HT<sub>3</sub> nanobody (VHH15, gift from H. Nury, Institut de Biologie structurale) was engineered to include a carboxy-terminal fusion with mCherry-His6 through a SSGSS linker and a gp64 signal peptide sequence was appended to the amino terminus to facilitate secretion into the insect cell culture medium. The resultant plasmid, pFastBac-gp64-VHH15-mCherry-His6, was used to transfect Sf9 cells, generating P1 virus. Sf9 cells were then infected with amplified P2 virus for nanobody expression and collected at 60 h after infection. The culture was centrifuged at 3,500g for 15 min and the supernatant was filtered through a 0.22 μm filter. The filtered supernatant was adjusted to pH 7.5 using 1 M HEPES (pH 8.0), and divalent ions were replenished by adding 5 mM CaCl<sub>2</sub> and 2 mM NiSO<sub>4</sub>. The supernatant was then incubated with 2 ml of Ni-NTA resin for 2 h at 4 °C. The resin was washed in batch with 5 column volumes of VHH15 buffer (500 mM NaCl and 50 mM Tris (pH 8.0)), then loaded onto a column and further washed with 5 column volumes of VHH15 buffer with 20 mM imidazole.

The column was then eluted with 3 column volumes of elution buffer (125 mM NaCl, 250 mM imidazole and 50 mM Tris (pH 7.4)). The elute was concentrated and loaded onto a Superdex 200 10/30 (GE Healthcare) gel filtration column in the buffer 10 mM HEPES (pH 7.5) and 100 mM NaCl. Fractions containing the peak were pooled and concentrated to 10 μM (0.39 mg ml<sup>-1</sup>).

#### Histology and immunostaining

Immunofluorescence imaging in the small and large intestine was performed using 10 μm cryosections. Blocking was performed with 5% w/v BSA (Sigma), 5% normal serum corresponding to secondary antibody species and 0.3% Triton-X in PBS at room temperature for 30 min. Primary antibodies were incubated overnight at 4 °C at the indicated dilutions. Antibodies used were against serotonin (1:5,000, Immunostar), TUJ1 (1:500, Abcam), collagen IV (1:500 Abcam), cleaved caspase-3 (Asp175) (1:500, Cell Signaling Technology), lysozyme (1:1000, Agilent), GFP (1:500, Abcam) and mCherry (1:500, Takara). Secondary antibodies from Invitrogen (Alexa Fluor 647 goat anti-rabbit, Alexa Fluor 568 goat anti-rabbit and Alexa Fluor 488 goat anti-chicken) were incubated at 1:500 dilution for 2 h at room temperature at 1:500 dilution. Z stack images were taken with a Nikon CSU-W1 spinning disk confocal microscope as described above (UCSF Center for Advanced Light Microscopy). Maximum-intensity projections were generated using Fiji (v.2.14).

#### Whole-mount staining of EC cells and mucosal nerve fibres

A piece of the jejunum was isolated from 8–16-week-old *Pirt1<sup>Cre</sup>;Ai14* mice. *Pirt1<sup>Cre</sup>;Ai14* mice were used because of the high expression level of tdTomato in mucosal nerve fibres. Isolated tissue samples were washed, dissected open and fixed with 4% PFA for 4 h at 4 °C. Blocking was performed with 5% w/v BSA (Sigma), 5% donkey serum and 0.3% Triton-X in PBS at room temperature for 3 h. Tissue samples were then incubated in a primary antibody solution (1:500 rabbit anti-serotonin (Immunostar) and 1:500 goat anti-collagen IV (Abcam)) for 2 days at 4 °C. Following primary incubation, tissue samples were washed 3 times in PBS with 0.2% Triton-X and incubated overnight in a secondary antibody solution (1:500 Alexa Fluor 488 donkey anti-rabbit and Alexa Fluor 647 donkey anti-goat). After overnight incubation, tissue samples were washed 3 times in PBS with 0.2% Triton-X and mounted with ProLong Diamond antifade mountant. Z stack images were taken with a Nikon CSU-W1 spinning disk confocal microscope as described above, using a Plan Apo VC ×100/1.4 oil objective (UCSF Center for Advanced Light Microscopy). Image deconvolution and 3D image reconstruction were conducted using Huygens (Scientific Volume Imaging) and Imaris (Oxford Instruments), respectively. The distances between the basolateral side of EC cells and the nearest dendrites were manually measured using Imaris.

#### Immunostaining of HEK293T cells with the 5-HT<sub>3</sub> nanobody

HEK293T cells were plated on 4-well chamber slides (Ibidi) and transfected with either pcDNA3-5-HT<sub>3A</sub> or the empty pcDNA3 plasmid. After overnight incubation, cells were fixed with 4% PFA for 20 min at room temperature. Fixed cells were incubated with VHH15-mCherry in PBS and 0.1% Triton-X (1:20 dilution) for 1 h at room temperature. After staining, cells were washed with PBS and 0.1% Triton-X 3 times and mounted with ProLong Diamond antifade mountant. Z stack images were taken with a Nikon CSU-W1 spinning disk confocal microscope as described above (UCSF Center for Advanced Light Microscopy). Maximum-intensity projections were generated using Fiji (v.2.14).

#### Nodose and dorsal root ganglia isolation and immunostaining with the 5-HT<sub>3</sub> nanobody

Nodose ganglia and dorsal root ganglia (DRG) were collected from both male and female *Htr3a<sup>eGFP</sup>* mice between 8 and 16 weeks of age. The dissected ganglia were fixed in 4% PFA for 3 h at 4 °C. Blocking was

## Article

performed with 5% w/v BSA (Sigma), 5% goat serum and 0.3% Triton-X in PBS at room temperature for 3 h. The DRG were then incubated with VHH15-mCherry (1:20 dilution) in PBS with 0.1% Triton-X overnight at 4 °C. After incubation, the ganglia were briefly washed in PBS and fixed again in 4% PFA for 30 min at 4 °C. Following a PBS wash, ganglia were transferred to a primary antibody solution (1:500 chicken anti-GFP (Abcam) and 1:500 rabbit anti-mCherry (Takara)) overnight. Ganglia were then washed 3 times in PBS with 0.2% Triton-X and transferred to a secondary antibody solution overnight (1:500 Alexa Fluor 488 goat anti-chicken and Alexa Fluor 568 goat anti-rabbit). The stained ganglia were then washed 3 times in PBS with 0.2% Triton-X and mounted with ProLong Diamond antifade mountant. Z stack images were taken with a Nikon CSU-W1 spinning disk confocal microscope as described above (UCSF Center for Advanced Light Microscopy). Maximum-intensity projections were generated using Fiji (v.2.14).

### Immunostaining of the intestine with the 5-HT<sub>3</sub> nanobody

The jejunum and proximal colon were collected from male and female *Htr3a<sup>eGFP</sup>* mice between 8 and 16 weeks of age. Tissue samples were dissected open, washed and incubated in staining buffer containing VHH15-mCherry (1:30 dilution) and protease inhibitor cocktail (Roche) in Krebs buffer for 2 h at room temperature. After staining, the tissue samples were washed 3 times with DPBS and fixed in 4% PFA for 1 h at room temperature. Blocking was performed with 5% w/v BSA (Sigma), 5% goat serum and 0.3% Triton-X in PBS at room temperature for 3 h. Tissue samples were then incubated in a primary antibody solution (1:500 chicken anti-GFP (Abcam) and 1:500 rabbit anti-mCherry (Takara)) for 2 days at 4 °C. Following incubation, the tissue samples were washed 3 times in PBS with 0.2% Triton-X and incubated in a secondary antibody solution (1:500 Alexa Fluor 488 goat anti-chicken and Alexa Fluor 568 goat anti-rabbit). After overnight incubation, the tissue samples were washed 3 times in PBS with 0.2% Triton-X and mounted with ProLong Diamond antifade mountant. Z stack images were taken with a Nikon CSU-W1 spinning disk confocal microscope as described above (UCSF Center for Advanced Light Microscopy). Maximum-intensity projections were generated using Fiji (v.2.14).

### In situ hybridization

Cryosections (5 or 10 µm) were prepared as described above. Single-molecule RNA-FISH was performed using a RNAscope Multiplex Fluorescent Detection Kit v.2 (Advanced Cell Diagnostics) according to the manufacturer's protocol. The following probes were used in this study: Mm-Tph1-C2 (318701-C2), Mm-Trpa1-C1 (512891), Mm-Trpm2-C1 (316831), Mm-Htr4-cust-C3 (408241-C3) and Mm-Olfm4-C1 (311831). Z stack images were taken with a Nikon CSU-W1 spinning disk confocal microscope as described above (UCSF Center for Advanced Light Microscopy). Maximum-intensity projections were generated using Fiji (v.2.14).

### GCaMP imaging using intestinal organoids

Five days after passage, *Tac1<sup>Cre</sup>;Polr2a<sup>(GCaMP5g-ires-tdTomato)</sup>* organoids were removed from Matrigel (Corning) and mechanically broken up with a 1,000 µl pipette. The organoid fragments were seeded onto Cell-Tak (Corning)-coated coverslips and placed in a recording chamber containing Ringer's solution (140 mM NaCl, 5 mM KCl, 2 mM CaCl<sub>2</sub>, 2 mM MgCl<sub>2</sub>, 10 mM D-glucose and 10 mM HEPES-Na (pH 7.4)). EC cells were identified by tdTomato expression. GCaMP imaging was performed with an upright microscope equipped with a Grasshopper 3 (FLIR) camera and a Lambda LS light source (Sutter). Organoids were maintained under a constant laminar flow of Ringer's solution applied by a pressure-driven microperfusion system (SmartSquirt, Automate Scientific). All pharmacological reagents were delivered by local perfusion. Acquired images were analysed using Fiji software (NIH). ROIs were drawn around individual EC cells and  $\Delta F/F_0$  values were calculated.

### Organoid swelling assay

Organoids were first passaged into organoid culture medium lacking *N*-acetylcysteine to prevent the inhibition of TRPA1 channels. At 24 h after passage, organoids were treated with 1 µM serotonin, 10 µM RS 23597-190 or 5 µM A967079 in *N*-acetylcysteine-free organoid culture medium. Images of the organoids were captured at 60 min after serotonin treatment and 12 h after A96 treatment. Cross-sectional areas of the organoids were subsequently measured using Fiji (v.2.14).

### Biosensor experiments

HEK293T cells transiently transfected with biosensor plasmids (gGRAB<sub>5-HT<sub>2m</sub></sub>, 5-HT<sub>2A</sub> receptor and GCaMP8m, 5-HT<sub>3</sub> channel, or gGRAB<sub>ATPL0</sub> sensor) were dissociated with trypsin and washed once with Ringer's solution. The dissociated cells were plated on top of intestinal organoids. Individual HEK293T cells were carefully lifted from coverslips and positioned 5 µm from an EC cell using a glass pipette. For the 5-HT<sub>3</sub> biosensor experiments, whole-cell configuration was achieved before lifting the cell. The membrane potential was held at -80 mV to measure inward 5-HT<sub>3</sub> currents. For 5-HT<sub>2A</sub> and gGRAB<sub>ATPL0</sub> biosensor experiments, imaging was performed using an upright microscope equipped with a Grasshopper 3 camera (FLIR) run using the Micro-Manager software (v.2.0) and a Lambda LS light source (Sutter Instrument). The entire area of each biosensor cell was used for the calculation of  $\Delta F/F_0$  values. For gGRAB<sub>5-HT<sub>2m</sub></sub> biosensor experiments, imaging was performed on a Leica SP8 confocal microscope with LAS X software (Leica Microsystems, v.3.5.5.19976). At the end of each recording, gGRAB<sub>5-HT<sub>2m</sub></sub> was fully activated with 500 µM serotonin. In these experiments, only the portion of each biosensor cell membrane within 5 µm of an EC cell was used for the calculation of  $\Delta F/F_0$  values, which were then normalized to the maximum signals activated by serotonin. In all the biosensor experiments, the bath solution was static to prevent the washout of endogenously released serotonin, and pharmacological agents were manually applied with a 1,000 µl pipette. All images were analysed using Fiji (v.2.14).

### Electrophysiology

Electrophysiological recordings were performed with an Axopatch 200B amplifier (Molecular Devices) connected to Digidata 1550B (Molecular Devices), which was connected to pClamp software (v.10.7), sampling at 10 kHz and filtering at 1 kHz. Membrane potentials were corrected for liquid junction potentials. Patch electrodes (3–6 MΩ) were pulled from borosilicate capillaries (BF-150-110-10, Sutter Instrument). The external solution for both EC cell and 5-HT<sub>3</sub> channel recordings was Ringer's solution. For TRPM2 recordings, the external solution contained 150 mM NaCl, 2 mM CaCl<sub>2</sub>, 1 mM MgCl<sub>2</sub>, 5 mM HEPES-Na (pH 7.4) and 10 mM D-glucose. The NMDG external solution was composed of 150 mM NMDG-Cl, 2 mM CaCl<sub>2</sub>, 1 mM MgCl<sub>2</sub>, 5 mM HEPES-Na (pH 7.4) and 10 mM D-glucose. The intracellular solution for EC cell recordings consisted of 140 mM K-aspartate, 13.5 mM NaCl, 1.6 mM MgCl<sub>2</sub>, 0.09 mM EGTA, 9 mM HEPES-K (pH 7.35), 14 mM phosphocreatine-tris, 4 mM MgATP and 0.3 mM Na<sub>2</sub>GTP. Intracellular solution for 5-HT<sub>3</sub> recordings consisted of 140 mM K-gluconate, 5 mM NaCl, 1 mM MgCl<sub>2</sub>, 10 mM EGTA-K and 10 mM HEPES-K (pH 7.2). For TRPM2 recordings, the intracellular solution included 150 mM NaCl, 5 mM HEPES-Na (pH 7.4), 5 mM EGTA-Na, 1 mM MgCl<sub>2</sub>, 5.1 mM CaCl<sub>2</sub> (producing a final free Ca<sup>2+</sup> concentration of 100 µM) and 500 µM ADP ribose (Sigma).

### EC cell dissociation

EC cells were isolated from the upper half of the small intestine of 8–16-week-old *Tac1<sup>Cre</sup>;Polr2a<sup>(GCaMP5g-ires-tdTomato)</sup>* mice. The tissue was cut into approximately 3 cm segments, incubated in 10 ml cold DPBS with 30 mM EDTA and 1.5 mM DTT on ice for 20 min, then transferred to 6 ml warm DPBS with 30 mM EDTA and incubated at 37 °C for 8 min. To

dissociate the epithelial layer, vigorous shaking was applied for 30–60 s. The dissociated epithelium was centrifuged and washed with DPBS containing 10% FBS. The washed epithelium was digested in 10 ml digestion buffer (HBSS with 0.3 mg ml<sup>-1</sup> dispase II (Sigma) and 0.2 mg ml<sup>-1</sup> DNaseI (Sigma)) at 37 °C for 8 min, with vigorous shaking at 2-min intervals. The cells were then washed once with HBSS containing 10% FBS and 0.2 mg ml<sup>-1</sup> DNaseI, filtered through 70 µm and 40 µm strainers, and resuspended in DMEM supplemented with 10% FBS, B27 and 5 µM Y-27632 (Sigma). Cells were plated onto glass coverslips precoated with 5% Matrigel solution. Two days after dissociation, EC cells exhibiting the characteristic polygonal or cone-shaped morphology were predominantly surviving cells from the crypt regions. These crypt-originating EC cells were subsequently used for electrophysiological recordings and GCaMP imaging conducted 2–3 days after dissociation.

### Intestinal $I_{sc}$ measurement in mice

The ileum was excised under anaesthesia and soaked in isoosmolar solution containing 300 mM mannitol and 10 µM indomethacin. The mucosa was stripped from serosa and muscle layers using a dissection microscope and mounted on Ussing chambers containing Ringer's solution (120 mM NaCl, 5 mM KCl, 1 mM CaCl<sub>2</sub>, 1 mM MgCl<sub>2</sub>, 10 mM D-glucose, 5 mM HEPES-Na (pH 7.4) and 25 mM NaHCO<sub>3</sub>) on the basolateral side. For the apical side, a similar solution was used except 120 mM NaCl was replaced with 60 mM NaCl and 60 mM sodium gluconate, and glucose was replaced with 10 mM mannitol. Compounds were added to both apical and basolateral bathing solutions unless specified otherwise. The solutions were aerated with 95% O<sub>2</sub> and 5% CO<sub>2</sub> and maintained at 37 °C during experiments.  $I_{sc}$  values were measured using an EVC4000 multichannel voltage clamp (World Precision Instruments) connected to pClamp software (v.10.7) using Ag–AgCl electrodes and 3 M KCl agar bridges as previously described<sup>64</sup>.

### Retrograde tracing of mucosal afferents from the proximal small intestine

Adult male mice of C57BL/6 background (Jackson Laboratory) aged 16–20 weeks were used. Retrograde tracing using cholera toxin subunit B (CTB, 0.5%) directly conjugated to Alexa Fluor 488 (Invitrogen, Thermo Fisher Scientific, C2284) was performed from the lumen of the proximal small intestine (jejunum) using a previously described method<sup>41</sup>, but with modifications. A small aseptic abdominal incision was made in mice anaesthetized with isoflurane (2–4% in oxygen). The proximal small intestine was located, and 5-µl injections were made through the intestinal wall into the lumen at 3 sites covering a length of 5 cm. The tracer was injected completely before the withdrawal of the needle back through the intestine wall, which was gently rubbed together using cotton tip applicators to distribute the tracer throughout the lumen. Injections were made with a 30-gauge needle (HAMC7803-07, point style: 4; Hamilton, Bio-Strategy) attached to a Hamilton 5 µl syringe (HAMC7634-01, 5 µl 700 series RN syringe; Hamilton, Bio-Strategy). The abdominal incision was then sutured closed, and analgesic (buprenorphine, 0.1 mg kg<sup>-1</sup>) and antibiotic (ampicillin, 50 mg kg<sup>-1</sup>) administration were given subcutaneously as mice regained consciousness. Mice were then individually housed and closely monitored for 4 days before the following experiments were performed: (1) perfusion and fixation, and collection of nodose and jugular ganglia (vagal ganglia) and spinal DRGs (T8–13) or removal of vagal ganglia for downstream dissociation; (2) cell picking and single cell RT-PCR; or (3) Ca<sup>2+</sup> imaging studies.

### CLARITY processing and imaging of sensory ganglia

The CLARITY method, which removes lipids to render tissue transparent while preserving the ultrastructure<sup>65–67</sup>, was used to visualize CTB-labelled neurons in intact whole nodose and DRGs. Four days after retrograde-tracing surgery, mice were euthanized by Lethobarb overdose (intraperitoneal administration) and underwent transcardial

perfusion and fixation as previously described<sup>67</sup>. Following removal of individual vagal ganglia and DRGs and post-fixation (24 h in 4% PFA at 4 °C), ganglia were placed in 4% PFA–hydrogel solution (4% acrylamide, 0.25% VA-044 in PBS, Sigma-Aldrich) at 4 °C for 48 h. Residual oxygen was then removed from samples, as oxygen inhibits hydrogel polymerization, using a standard vacuum pump and a desiccation chamber attached to a nitrogen gas supply<sup>65</sup>. Samples were degassed for 20 min and exposed to nitrogen gas for 5 min before transfer to a 37 °C oven until the hydrogel solution had uniformly polymerized (90 min). Samples were removed from the hydrogel and underwent passive clearing in 8% SDS and 200 mM boric acid solution (Sigma-Aldrich) at 37 °C. The buffer was changed after 24 h and again after 72 h, at which point samples were transparent. Ganglia were then placed individually (left and right) into wells filled with RapiClear 1.47 refractive index solution (RC147001, SunJin Lab) of a 18-well glass slide for at least 4 h before confocal microscopy. Fluorescence was visualized with a confocal laser scanning microscope (Leica TCS SP8X, Wetzlar). Images (1,024 × 1,024 pixels) were obtained with ×20 oil-immersion lenses and 495 nm excitation and 503/538 nm emission detection settings. Ganglia were optically sectioned (10–15 µm), and projected images were reconstructed for each ganglion (230–390 µm). Images were processed using Leica LAS Lite and ImageJ software. Labelled neurons were manually counted from digital photomicrographs of CLARITY-cleared ganglia using ImageJ Cell Counter tool. Data were collected from  $N = 4$  male mice,  $n$  from 2 ganglia per spinal level ( $n = 6$  NG and T8–T9 with 1 ganglion lost during tissue processing from  $N = 2$  mice and  $n = 7$  T10–T13 DRG with 1 ganglion lost during tissue processing from  $N = 1$  mouse).

### Calcium imaging of dissociated nodose ganglia neurons

Retrogradely traced nodose ganglion neurons were isolated from adult mice. In brief, 4 days after mucosal retrograde tracing, mice were euthanized by CO<sub>2</sub> inhalation and nodose ganglia were surgically removed and were digested with 4 mg ml<sup>-1</sup> collagenase II (Gibco, Life Technologies) and 4 mg ml<sup>-1</sup> dispase (Gibco) for 30 min at 37 °C, followed by 4 mg ml<sup>-1</sup> collagenase II for 10 min at 37 °C, similar to that previously described for DRGs<sup>4</sup>. Neurons were then mechanically dissociated into a single-cell suspension by trituration through fire-polished Pasteur pipettes. Neurons were resuspended in DMEM (Gibco) containing 10% FCS (Invitrogen), 2 mM L-glutamine (Gibco), 100 mM MEM non-essential amino acids (Gibco), 100 mg ml<sup>-1</sup> penicillin–streptomycin (Invitrogen) and 100 ng ml<sup>-1</sup> NGF (Sigma). Neurons were spot-plated on coverslips coated with poly-D-lysine (800 mg ml<sup>-1</sup>) and laminin (20 mg ml<sup>-1</sup>) and maintained at 37 °C in 5% CO<sub>2</sub>. After 24 h in culture, neurons were loaded with 2.5 µM Fura-2-AM (Thermo Fisher Scientific) and 0.02% (v/v) pluronic acid for 30 min at room temperature in Ringer's solution (NaCl 140 mM, KCl 5 mM, CaCl<sub>2</sub> 1.25 mM, MgCl<sub>2</sub> 1 mM, glucose 10 mM and HEPES 10 mM, pH 7.4). After a brief wash, coverslips were transferred to a recording chamber filled with Ringer's solution at room temperature (about 22 °C). Retrogradely traced nodose ganglion neurons were identified by the presence of the CTB-488 tracer and viability was verified by responses to 40 mM KCl. Fura-2-AM fluorescence was measured at 340 nm and 380 nm excitation, and 530 nm emission was measured using an Olympus IX71 microscope in conjunction with a Sutter Lambda 10-3 wavelength switcher and the Chroma filter set no. 49011 (ET480/40x (exciter), T510lpxxt (beamsplitter), ET535/50m (emitter)). Fluorescence images were obtained every 5 s using a ×4 objective with a monochrome CCD camera (Retiga ELECTRO). Images were taken at baseline and after administration of adenosine 5'-triphosphate disodium salt (ATP, 10 µM, Sigma Merck), *m*-chlorophenylbiguanide hydrochloride (mCPBG, 10 µM, Tocris), tegaserod maleate (1 µM, Sigma Merck), capsaicin (50 nM, Sigma Merck), allyl isothiocyanate (AITC, 1 µM, Sigma Merck), H<sub>2</sub>O<sub>2</sub> (200 µM, Sigma Merck) and KCl (40 mM). Fluorescence traces of cell bodies were extracted using Metafluor software (Molecular Devices). ROIs were manually drawn around the

cell bodies of neurons and their fluorescence traces were extracted as the 340/380 ratio.

## Single-cell RT-PCR on mucosal-traced nodose ganglion neurons

Four days after the mucosal retrograde-tracing procedure described above, nodose ganglia were removed and enzymatically dissociated. Neurons were allowed to settle for 2 h before adding 2 ml of medium and preparing the coverslips for single-cell picking. Traced cells were manually picked using a micromanipulator under a microscope equipped with an appropriate fluorescent filter. Cells were under a continuous slow flow of RNA/DNase-free PBS to reduce potential contamination. After picking a traced cell, the glass capillary was broken into a tube containing 9  $\mu$ l lysis buffer with 1  $\mu$ l DNaseI (TaqMan Gene Expression Cells-to-CT kit; Thermo Fisher Scientific). A bath control was taken and analysed from every coverslip with other samples. The whole-cell lysate was used for cDNA synthesis using SuperScript VIL0 master mix (Thermo Fisher Scientific) and diluted 1:5 for further PCR analysis. PCR was performed according to the manufacturer's instructions using TaqMan Gene Expression master mix (Thermo Fisher Scientific) for 55 cycles. A target was defined to be present when a typical amplification curve was produced. Predesigned Taqman probes were purchased from Thermo Fisher Scientific (*P2rx2*, Mm00462952\_m1; *P2rx3*, Mm00523699\_m1; *Htr3a*, Mm00442874\_m1; *Htr3b*, Mm00517424\_m1; *Htr4*, Mm00434129\_m1; *Trpv1*, Mm01246300\_m1; *Trpa1*, Mm01227437\_m1; and *Trpm2*, Mm00663098\_m1).

## Ex vivo mucosal recordings from sensory nerves innervating the small intestine

**Jejunum afferent preparation.** Male and female mice (12–18 weeks old) were euthanized by CO<sub>2</sub> inhalation. A 2 cm piece of the jejunum with intact mesentery segments was removed, opened longitudinally and pinned down (mucosal side up) in a specialized organ bath. The jejunum was perfused with a modified Krebs buffer (117.9 mM NaCl, 4.7 mM KCl, 25 mM NaHCO<sub>3</sub>, 1.3 mM NaH<sub>2</sub>PO<sub>4</sub>, 1.2 mM MgSO<sub>4</sub>, 2.5 mM CaCl<sub>2</sub> and 11.1 mM D-glucose), bubbled with carbogen (95% O<sub>2</sub>, 5% CO<sub>2</sub>) at 34 °C. Krebs buffer also contained 1  $\mu$ M nifedipine (to suppress smooth muscle activity) and 3  $\mu$ M indomethacin (to suppress potential inhibitory actions of endogenous prostaglandins). The free end of the segment of mesentery was extended into an adjacent recording compartment, which was subsequently filled with paraffin oil. A whole nerve bundle supplying the jejunal segment was then located within the mesentery, carefully cleaned away and placed on a platinum-recording electrode. Action potentials (APs) generated within the jejunum travelled across the nerve fibres, through the recording electrode, into a differential amplifier, filtered, sampled (20 kHz) using a 1401 interface (CED) run by Spike 2 software (v.5.18) and stored on a PC for offline analysis.

**Optogenetic stimulation of mucosal afferents.** *Scn10a<sup>Cre</sup>;Rosa26<sup>(lsl-ChR2)</sup>* mice, which express ChR2 in sensory afferents but not EC cells were used<sup>4,68</sup>. This transgenic line enabled us to optogenetically activate mucosal afferents in an EC-independent and mechanically independent manner, as previously described<sup>13</sup>. Using the jejunum ex vivo afferent preparation described above, we recorded the APs generated by stimulating a small section of the jejunum (about 3 mm<sup>2</sup>) with continuous exposures of increasing light (470 nm) intensities, ranging from 0.082 to 7 mW. This range of light intensities enabled us to determine the light-activation threshold of afferents and their stimulus-response profiles to graded light stimuli. We selectively identified mucosal afferents based on their lower optogenetic (and mechanical) stimulation thresholds<sup>13,69</sup>. Each light exposure was applied for 2 s with a 10-s interval between exposures. Light was delivered using a high power fibre-coupled LED light source (model BLS-FCS-0470-10) and multimode fibre patchcords (numerical aperture of 0.39 NA, core size of 400  $\mu$ m; FPC-0400-39-025MA-BP, Mightex). In selected experiments,

we perfused the section of the jejunum receiving the light stimuli with the TRPM2 agonist H<sub>2</sub>O<sub>2</sub> (200  $\mu$ M) or with the TRPA1 agonists AITC (100  $\mu$ M) or acrolein (100  $\mu$ M). These agonists were perfused alone or in the presence of the 5-HT<sub>3</sub> antagonist alosetron (10  $\mu$ M) or with the P2X antagonist PPADS (10  $\mu$ M). In selected experiments, we perfused the area receiving the light stimuli with 1  $\mu$ M of the 5-HT<sub>4</sub> antagonist RS 23597-190. A gravity-driven perfusion system slowly delivered the perfusion compounds. At 5 min after perfusion of these compounds, we repeated the illumination protocol (still under continuous perfusion of the compounds) at the increasing light intensities described above. APs generated throughout the recordings were analysed offline using the Spike 2 wavemark function and discriminated as single units based on a distinguishable waveform, amplitude and duration (CED). Data were expressed as follows: (1) the activity of the afferent induced by the compound tested or by individual light stimulus (AP per s); or (2) the light intensity threshold for AP activation (mW mm<sup>-2</sup>). *n* represents the number of afferents and *N* represents the number of animals analysed for each study. Data were analysed to determine whether they were distributed normally using D'Agostino–Pearson or Anderson–Darling tests, with subsequent analysis using two-way ANOVA with Šidák's multiple comparisons test (for more than two groups). For comparison between two groups, we used Wilcoxon matched-pairs signed rank tests or two-sided paired *t*-tests, or two-sided unpaired *t*-tests. A *P* value of  $\leq 0.05$  was considered significant.

**AP recording induced by optogenetic stimulation of EC cells.** For this experiment, we used a transgenic mouse line that expresses the light-sensitive protein ChR2 in EC cells (*Tph1<sup>CreER</sup>;Rosa26<sup>(lsl-ChR2)</sup>*), and the control counterpart line *Rosa26<sup>(lsl-ChR2)</sup>*. This enabled us to optogenetically activate EC cells in an agonist-independent manner. Using the jejunum ex vivo afferent preparation described above, we recorded the spontaneous nerve activity (baseline firing rate) of small intestinal afferents innervating the jejunum. Following 5 min of baseline recordings, a section of the jejunum (about 3 mm<sup>2</sup>) was illuminated with a light wavelength of 470 nm, at 100% intensity (equivalent to 7 mW<sup>-2</sup>), using a BioLED control module (model BLS-PL04-US) coupled with a high power fibre-coupled LED light source (model BLS-FCS-0470-10) and multimode fibre patchcords (numerical aperture of 0.39 NA, core size of 400  $\mu$ m; FPC-0400-39-025MA-BP, Mightex). We first applied pulses of light (3  $\times$  20 ms pulses at 5 Hz) and then continuous illumination (3  $\times$  20 s continuous light). For selected experiments, we perfused the section of the jejunum receiving the light stimuli with either alosetron (10  $\mu$ M) or PPADS (10  $\mu$ M), or a combination of both alosetron and PPADS (10  $\mu$ M each). Perfusion of these inhibitors was applied by a gravity-fed perfusion system, 5 min before light stimulation. Afferents sensitive to light are defined as follows: afferents in which the firing rate (AP per s) after light is more than double that of the firing rate (AP per s) at baseline. To quantify the effect of the abovementioned inhibitors on light-induced activation, we calculated the percentage of afferents 1) activated by light stimulation or 2) with enhanced firing rates after light stimulation at baseline and after application of the respective antagonists. *n* represents the number of afferents and *N* represents the number of animals analysed for each study. Significant differences in the data were determined using Chi-Squared tests and *t*-tests. A *P* value of  $< 0.05$  was considered significant.

## Analysis of scRNA-seq datasets

For mouse gut epithelial cells, we downloaded the normalized scRNA-seq data (GSE224223)<sup>20</sup> from the Gene Expression Omnibus (GEO) database, for which both epithelial and enteroendocrine cell subtypes are well annotated. For the mouse ENS, we downloaded the P21 mouse scRNA-seq data (GSM4504450)<sup>29</sup> from the GEO database and further performed normalization and annotation based on the original publication. All expression profiling were performed using Seurat 5.0.1. (Satija Laboratory, <https://satijalab.org/seurat/>) on R 4.4.1.

## Statistical analysis

Data were analysed using Prism (Graphpad) and  $n$  represents the number of cells, crypts, villi or independent experiments. Data were considered significant if  $P \leq 0.05$  using paired or unpaired two-sided Welch's  $t$ -tests, Mann–Whitney  $U$ -tests, one-way ANOVA, two-way ANOVA, Kruskal–Wallis tests, Wilcoxon matched-pairs signed rank tests or Chi-square tests. Statistical parameters are described in figure legends. All significance tests were justified considering the experimental design and we assumed normal distribution and variance, as is common for similar experiments. Sample sizes were chosen on the basis of the number of independent experiments required for significance and technical feasibility.

## Inclusion and ethics statement

We support inclusive, diverse and equitable conduct of research.

## Reporting summary

Further information on research design is available in the Nature Portfolio Reporting Summary linked to this article.

## Data availability

All data generated or analysed during this study are included in the manuscript and Supplementary Information. Reagents used here are available upon request. Source data are provided with this paper.

## Code availability

Custom codes were not generated in this study.

- Sei, Y. et al. Mature enteroendocrine cells contribute to basal and pathological stem cell dynamics in the small intestine. *Am. J. Physiol. Gastrointest. Liver Physiol.* **315**, G495–G510 (2018).
- Sato, T. et al. Single Lgr5 stem cells build crypt–villus structures in vitro without a mesenchymal niche. *Nature* **459**, 262–265 (2009).
- Edelstein, A. D. et al. Advanced methods of microscope control using µManager software. *J. Biol. Methods* **1**, e10 (2014).
- de Souza Goncalves, L. et al. Mg<sup>2+</sup> supplementation treats secretory diarrhea in mice by activating calcium-sensing receptor in intestinal epithelial cells. *J. Clin. Invest.* **134**, e171249 (2024).

- Tomer, R., Ye, L., Hsueh, B. & Deisseroth, K. Advanced CLARITY for rapid and high-resolution imaging of intact tissues. *Nat. Protoc.* **9**, 1682–1697 (2014).
- Grundt, L. et al. Chronic linaclotide treatment reduces colitis-induced neuroplasticity and reverses persistent bladder dysfunction. *JCI Insight* **3**, e121841 (2018).
- Wang, Q. et al. Comparative localization of colorectal sensory afferent central projections in the mouse spinal cord dorsal horn and caudal medulla dorsal vagal complex. *J. Comp. Neurol.* **532**, e25546 (2024).
- Hockley, J. R. F. et al. Single-cell RNAseq reveals seven classes of colonic sensory neuron. *Gut* **68**, 633–644 (2019).
- Brierley, S. M., Jones, R. C. 3rd, Gebhart, G. F. & Blackshaw, L. A. Splanchnic and pelvic mechanosensory afferents signal different qualities of colonic stimuli in mice. *Gastroenterology* **127**, 166–178 (2004).

**Acknowledgements** We thank J. Poblete for her technical support; J. Bayrer, H. Ingraham and all members of the Julius Laboratory for discussions; H. Nury for sharing the VHH15 plasmid; C. Bertozzi for sharing the StcE plasmid; J. L. Merchant for sharing the *Tph1<sup>CreER</sup>* mouse line; and staff at UCSF's core facilities, including the Center for Advanced Light Microscopy (D. Larsen, K. Herrington and S. Y. Kim, S10 Shared Instrumentation grant 1S10OD017993-01A1 for the Nikon CSU-W1 spinning disk confocal microscope). Illustrations in Figs. 1a–c, 2d,g,j, 3g, 5c,e and 6 and Extended Data Figs. 1a, 4b,d, 7c, 8c, 9a were created using BioRender (<https://biorender.com>). This work was supported by NIH grants NS105038, NS113869 and DK135714 to D.J.; BRAIN Initiative 1U01NS113358 and 1U01NS120824 to Y.L.; DK126070, DK072517 and EY036139 to O.C.; the National Natural Science Foundation of China (31925017 to Y.L.); the New Cornerstone Science Foundation through the New Cornerstone Investigator Program and the XPLOER PRIZE to Y.L.; a National Health and Medical Research Council (NHMRC) of Australia Investigator Leadership Grant (APP2008727) to S.M.B.; a NHMRC Ideas Grant (APP2029332) to J.C.; and the Cystic Fibrosis Foundation to O.C. K.K.T. was supported by a Damon Runyon Cancer Research Foundation Fellowship (DRG-(2387-30)). J.X. was supported by a Larry L. Hillblom Fellowship Grant (2024-A-044-FEL).

**Author contributions** Research design: K.K.T., O.C., S.M.B., Y.L. and D.J. Writing: K.K.T. and D.J., with input from all authors. Patch-clamp recordings of EC cells: K.K.T. and N.D.R. Development of serotonin sensors: F.D. Ussing chamber experiments: T.C. Jejunal afferent recordings: J.C. Mucosal retrograde tracings: A.M.H. Real-time PCR and analyses: S.G.-C. Ca<sup>2+</sup> imaging and analyses of vagal neurons: M.B. and T.O. Analyses of scRNA-seq datasets: J.X. All other experiments and analyses: K.K.T. Supervision of trainees: O.C., S.M.B., Y.L. and D.J. Project administration: K.K.T., O.C., S.M.B., Y.L. and D.J.

**Competing interests** D.J. is a scientific advisor to Rapport Therapeutics.

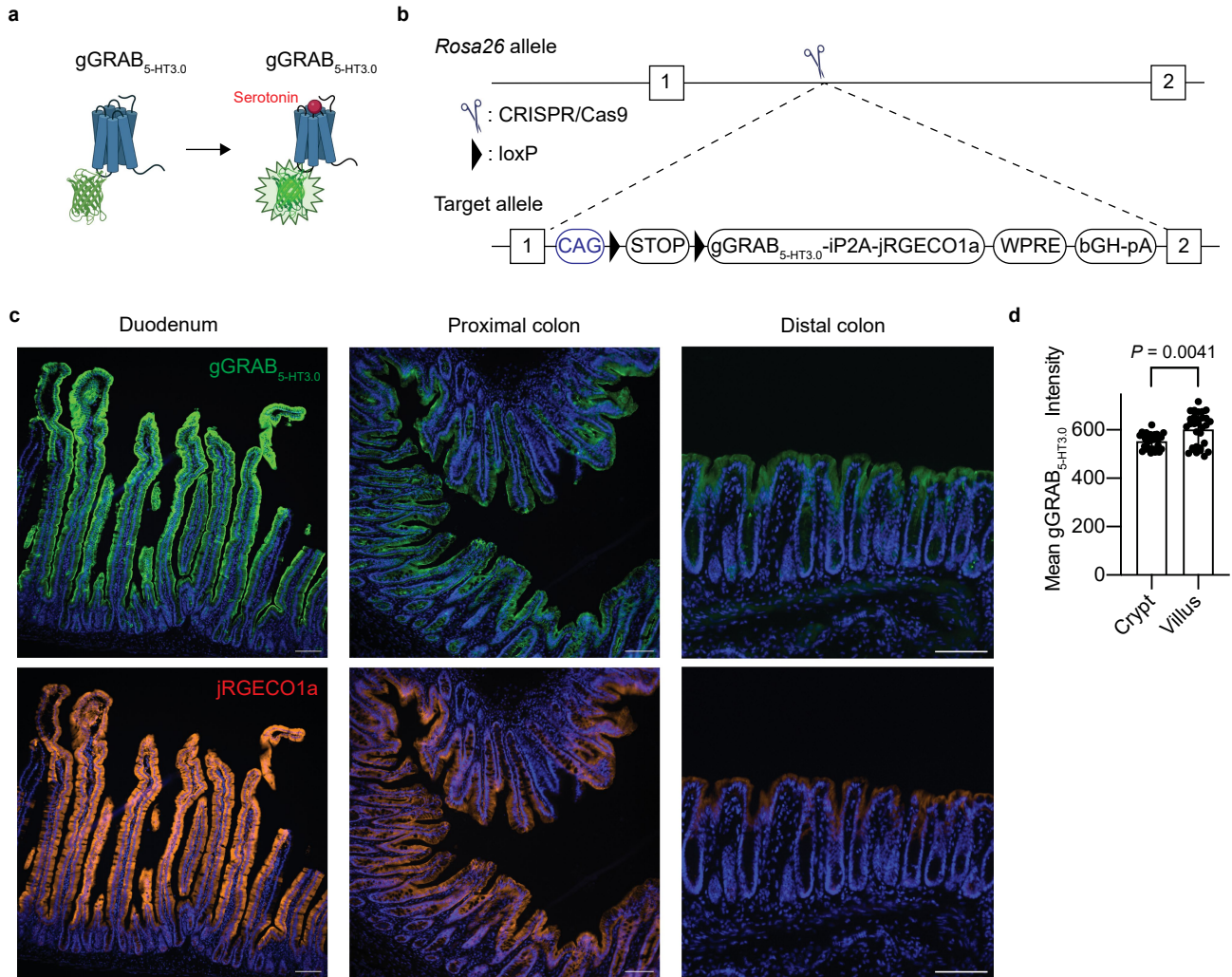
## Additional information

**Supplementary information** The online version contains supplementary material available at <https://doi.org/10.1038/s41586-024-08581-9>.

**Correspondence and requests for materials** should be addressed to Kouki K. Touhara, Stuart M. Brierley, Yulong Li or David Julius.

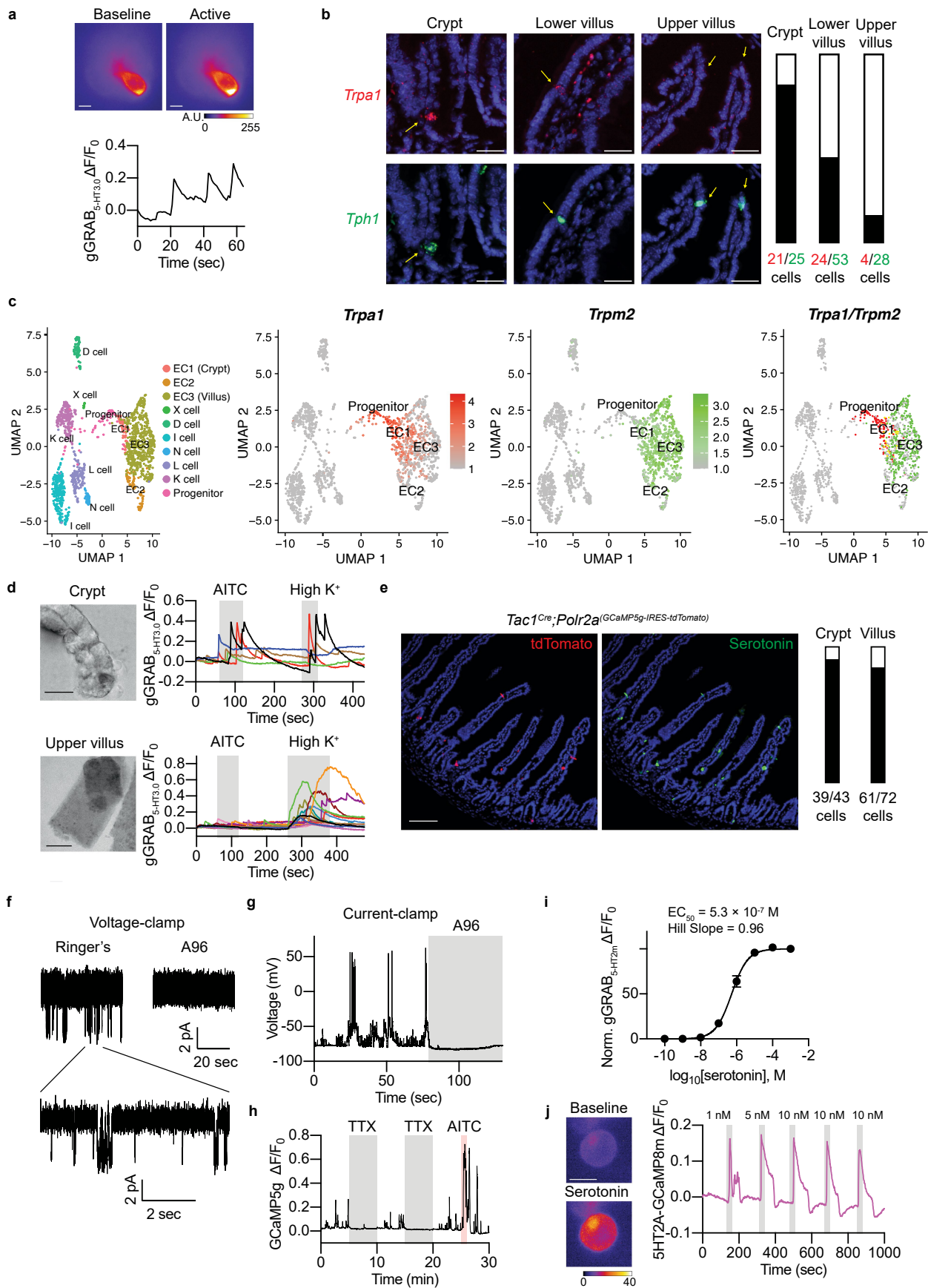
**Peer review information** *Nature* thanks Virginia Pedicord, Christoph Thaiss and the other, anonymous, reviewer(s) for their contribution to the peer review of this work. Peer reviewer reports are available.

**Reprints and permissions information** is available at <http://www.nature.com/reprints>.



**Extended Data Fig. 1 | Development and validation of the gGRAB<sub>5-HT3.0</sub> mouse model for detecting gut serotonin.** (a) gGRAB<sub>5-HT3.0</sub> is a modified metabotropic 5-HT receptor fused to cpEGFP. Upon serotonin binding, the receptor changes its conformation, leading to an increase in the fluorescent intensity of cpEGFP. (b) Strategy to generate the transgenic knock-in mouse line expressing gGRAB<sub>5-HT3.0</sub> and jRGECO1a in the *Rosa26* locus. (c) Immunohistochemical labeling of gGRAB<sub>5-HT3.0</sub> and jRGECO1a in

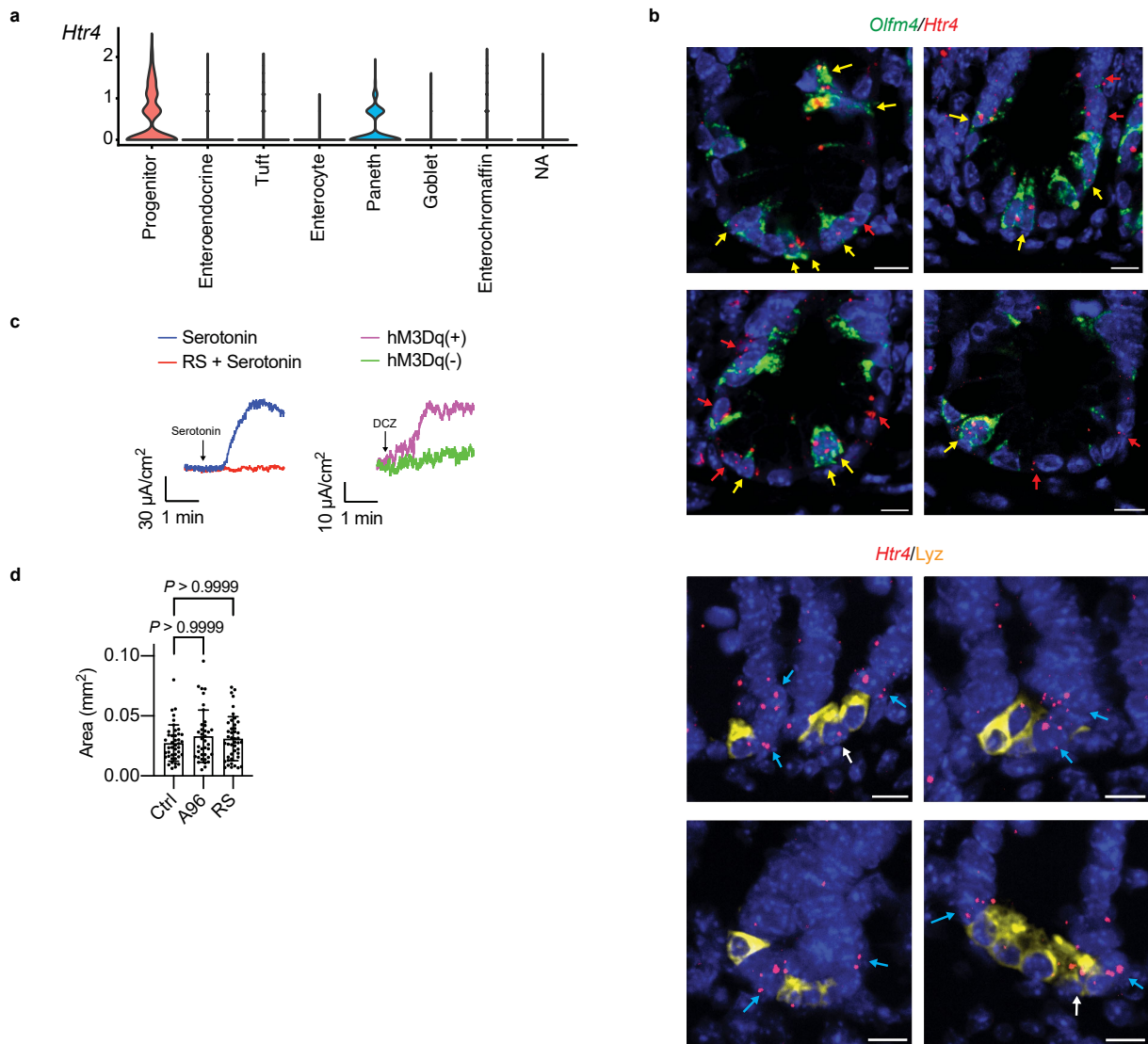
*Vil1<sup>Cre</sup>;Rosa26<sup>(gGRAB<sub>5-HT3.0</sub>-iP2A-jRGECO1a)</sup>* mice. gGRAB<sub>5-HT3.0</sub> and jRGECO1a were immunostained with an anti-GFP and anti-mCherry antibody, respectively. Scale bar = 100 μm, with each experiment repeated three times. (d) Expression of gGRAB<sub>5-HT3.0</sub> was quantified in crypts and villi. The average intensity was 553 ± 31 for crypts and 601 ± 67 for villi. Mean ± s.d., two-sided Mann-Whitney U test. n = 30 crypts or villi. The illustration in (a) was created using BioRender (<https://www.biorender.com>).



Extended Data Fig. 2 | See next page for caption.

**Extended Data Fig. 2 | TRPA1 drives tonic serotonin release from crypt EC cells.** (a) Spontaneous serotonin release in dissociated crypts from gGRAB<sub>5-HT3.0</sub> mice. Scale bar = 5  $\mu$ m, with the experiment repeated three times with similar results. (b) In situ hybridization of *Trpa1* and *Tph1* in the small intestine. *Tph1* is the rate-limiting enzyme in the serotonin synthesis that is expressed in EC cells in both crypts and villi. *Trpa1* expression is predominantly limited to the crypts and lower villi. Bars indicate the ratio of *Trpa1*-positive cells/*Tph1*-positive cells. Quantification was performed using tissue samples from 3 independent animals. Scale bar = 30  $\mu$ m. (c) UMAP showing major enteroendocrine cell (EEC) subtypes. Middle, gradient expression patterns of *Trpa1* (red) and *Trpm2* (green) are observed in crypt (EC1) versus villus (EC3) EC cells. Right, *Trpa1*<sup>+</sup> (red, expression threshold >1.5), *Trpm2*<sup>+</sup> (green, expression threshold >1.5), and double-positive (yellow) EC cells are all present. Enteroendocrine cell scRNA-seq data was downloaded and reanalyzed from GEO: GSE224223, using the same UMAP coordinates as in the original publication<sup>20</sup>. (d) AITC activates crypt but not upper villus EC cells in primary isolated crypts and villi from

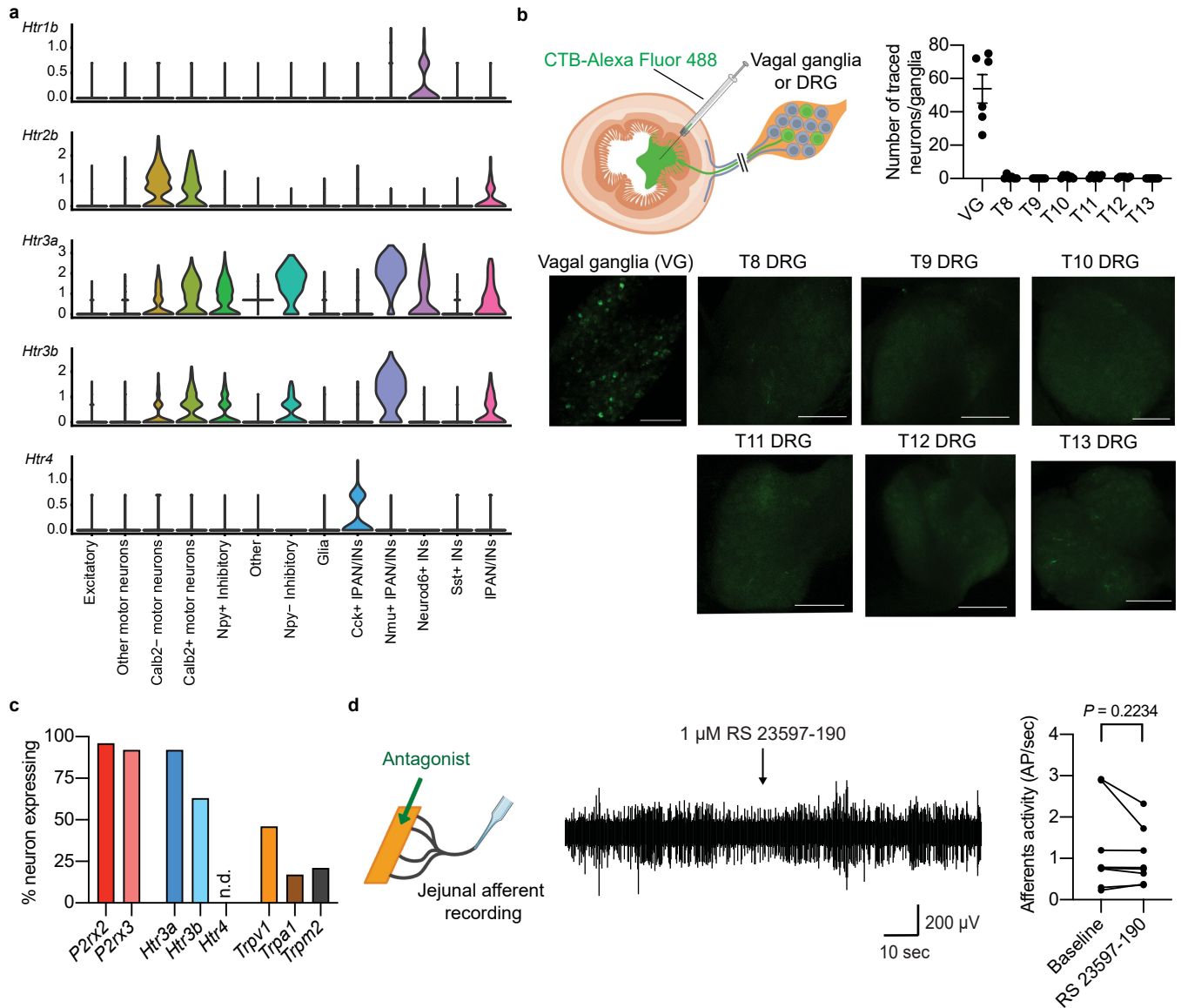
gGRAB<sub>5-HT3.0</sub> mice. Each colored trace represents an individual crypt or villus. Scale bar = 30  $\mu$ m. (e) Immunohistochemical labeling of crypt and villus EC cells in *Tac1*<sup>Cre</sup>;*Polr2a*<sup>(GCaMP5g-IRE5-tdTomato)</sup> mice. Bars indicate the ratio of tdTomato-positive cells/serotonin-positive cells. Scale bar = 100  $\mu$ m, with each experiment repeated three times. (f) A96-sensitive spontaneous TRPA1 channel opening in a primary dissociated crypt EC cell. The membrane potential was held at -80 mV. (g) In the same cell, A96 inhibits the spontaneous action potentials. 10  $\mu$ M A96 was applied as indicated above the signal. (h) 300 nM Tetrodotoxin (TTX) inhibits the spontaneous GCaMP activity of EC cells. (i) Normalized dose-response curve of gGRAB<sub>5-HT2m</sub> for serotonin in HEK cells in the presence of 1  $\mu$ M citalopram, a serotonin transporter inhibitor ( $EC_{50} = 5.3 \times 10^{-7}$  M, Hill Slope = 0.96, n = 10). (j) GCaMP imaging of HEK cells expressing 5-HT<sub>2A</sub> receptors and GCaMP8m. The biosensor cells repeatedly responded to 1–10 nM serotonin, with each experiment repeated three times with similar results. Scale bar = 10  $\mu$ m.



**Extended Data Fig. 3 | Expression of 5-HT<sub>4</sub> receptors in crypts.** (a) The expression pattern of *Htr4* in mouse gut epithelial cells, using the annotation provided by the original publication<sup>20</sup>. NA: not assigned. (b) (Top) In situ hybridization of *Htr4* (red) and *Olfm4* (green) in the small intestine. *Olfm4* is a specific marker for active intestinal stem cells at the crypt base. Yellow and red arrows indicate *Htr4*(+)/*Olfm4*(+) and *Htr4*(+)/*Olfm4*(-) cells, respectively. (Bottom) In situ hybridization of *Htr4* (red) and immunostaining of Lyz (yellow) in the small intestine. Lyz is a specific marker for Paneth cells at the crypt base. White and light blue arrows indicate *Htr4*(+)/Lyz(+) and *Htr4*(+)/Lyz(-) cells, respectively. Scale bar = 10  $\mu\text{m}$ , with each experiment repeated three times

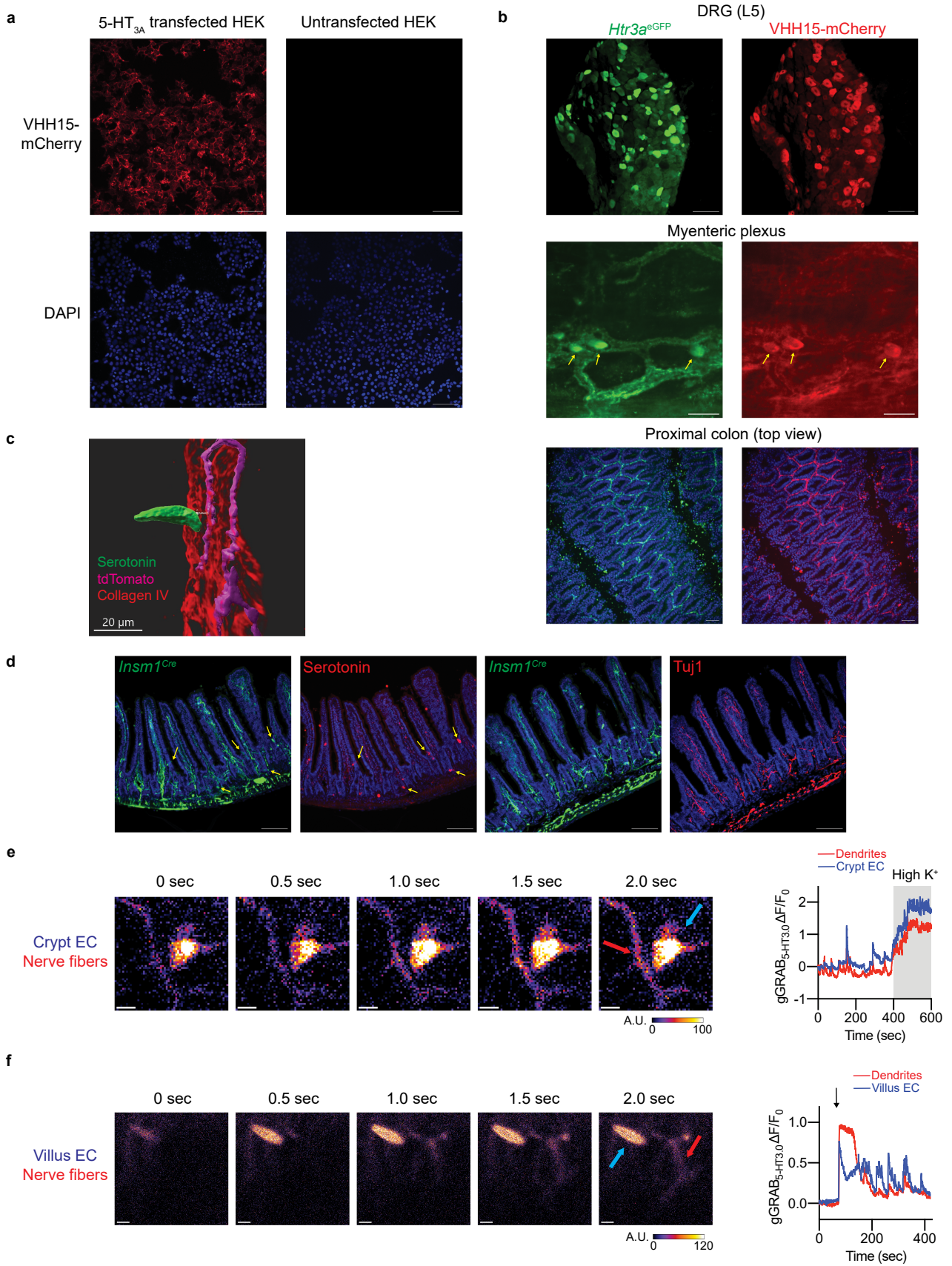
with similar results. (c) Ion secretion in ex vivo intestinal preparations was measured using the Ussing chamber. (Left) Time course of short-circuit currents ( $I_{sc}$ ) in response to 1  $\mu\text{M}$  serotonin with or without the 5-HT<sub>4</sub> antagonist (1  $\mu\text{M}$  RS 23597-190). (Right) Time course of short-circuit currents ( $I_{sc}$ ) in response to the DREADD receptor agonist, 1  $\mu\text{M}$  DCZ, in the ileal mucosa isolated from *Tac1<sup>Cre</sup>;ePet-Flp*;RC::FL-hM3Dq (hM3Dq(+)) or hM3Dq(-) control mice. (d) Intestinal organoids were grown in the presence of 5  $\mu\text{M}$  A96 or 10  $\mu\text{M}$  RS for 4 days, and cross-sectional areas were compared between untreated organoids. Mean  $\pm$  s.d., Kruskal-Wallis test followed by Dunn's multiple comparisons test. n = 42, 38, and 44 organoid per group.

# Article



**Extended Data Fig. 4 | Expression pattern of 5-HT<sub>3</sub> receptors in intrinsic and extrinsic gut sensory neurons.** (a) Expression patterns of all 5-HT receptor genes that can be detected in the mouse enteric nervous system (ENS) by scRNA-seq<sup>29</sup>. Nmu+ IPANs/INs represents mucosa-innervating intrinsic primary afferent neurons. ENS scRNA-seq data was downloaded and reanalyzed from GEO: GSM4504450. IN, interneurons; IPAN, intrinsic primary afferent neurons. (b) (Top left) Green fluorescent-conjugated cholera toxin B (CTB) retrograde tracer was injected into the small intestine lumen to specifically trace mucosal afferents while excluding fibres innervating the muscle layer. (Top right) Quantification of the number of AlexaFluor (AF)-488-labeled neurons within individual whole vagal ganglia (VG) and dorsal root ganglia (DRG, spinal levels thoracic T8 through to T13) 4 days following CTB-AF488 injection into the small intestine lumen. Data points represent the total

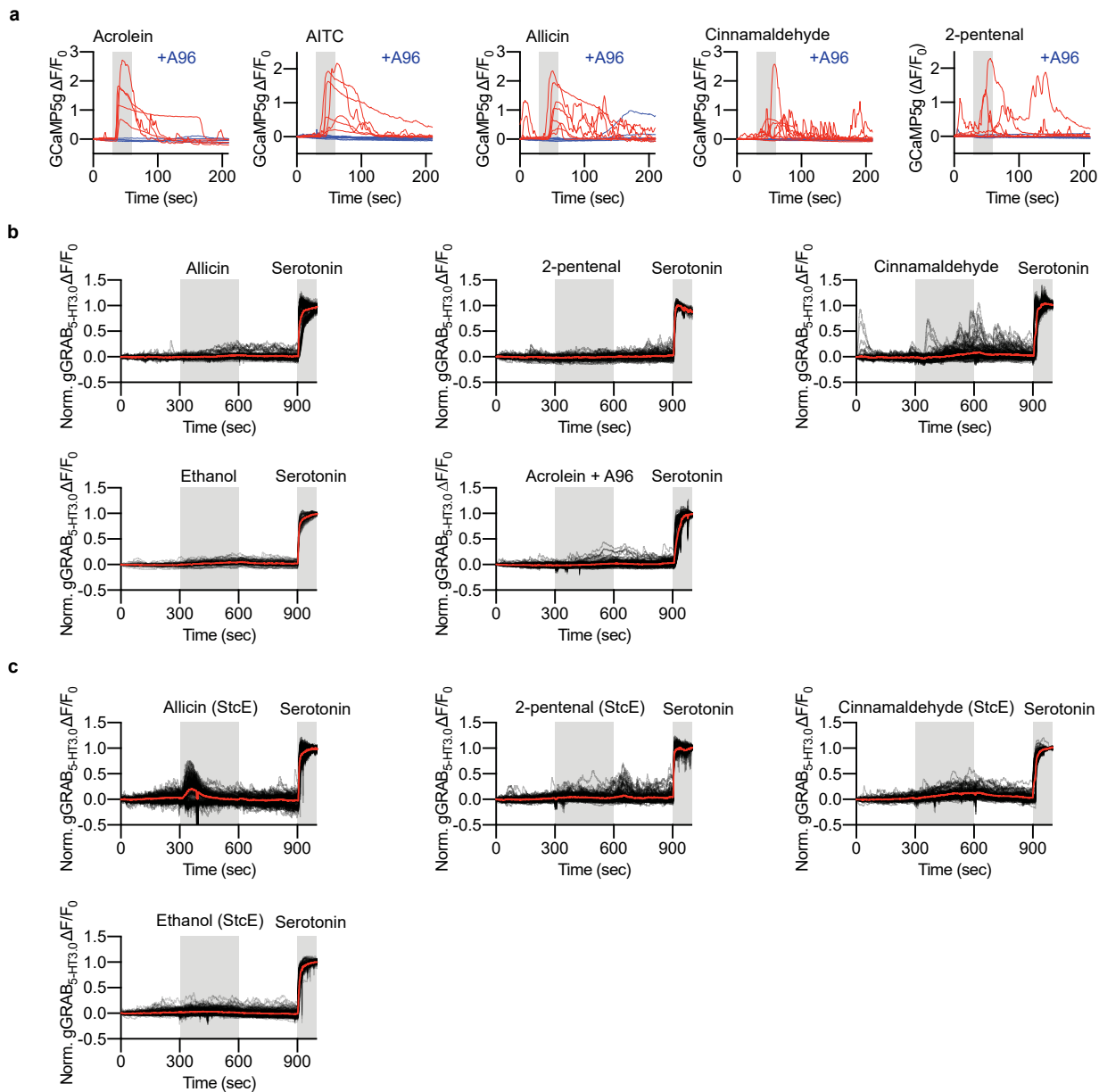
number of AF488-labeled neurons within individual ganglion, with  $n = 6-7$  ganglia/level  $\pm$  S.D;  $N = 4$  animals. (Bottom) Representative photomicrographs of CLARITY-cleared whole VG and DRG at T8, T9, T10, T11, T12, and T13. Scale bars = 150  $\mu$ m. Photomicrographs are maximum z-projection reconstructions from confocal-collected optical sections. (c) Single-cell RT-PCR analysis of retrogradely traced small intestine mucosa-innervating vagal neurons. A target was defined to be present when a typical amplification curve was produced.  $n = 24$  neurons;  $N = 3$  animals. (d) (Left) Schematic of ex vivo 'flat sheet' recordings from afferents innervating the jejunum. (Middle) A representative jejunal afferent recording before and after application of 1  $\mu$ M RS 23587-190. (Right) The number of action potentials is compared before and after application of 1  $\mu$ M RS 23597-190. Two-sided paired t-test.  $n = 8$  recordings. The illustration in (b) was created using BioRender (<https://www.biorender.com>).



**Extended Data Fig. 5** | See next page for caption.

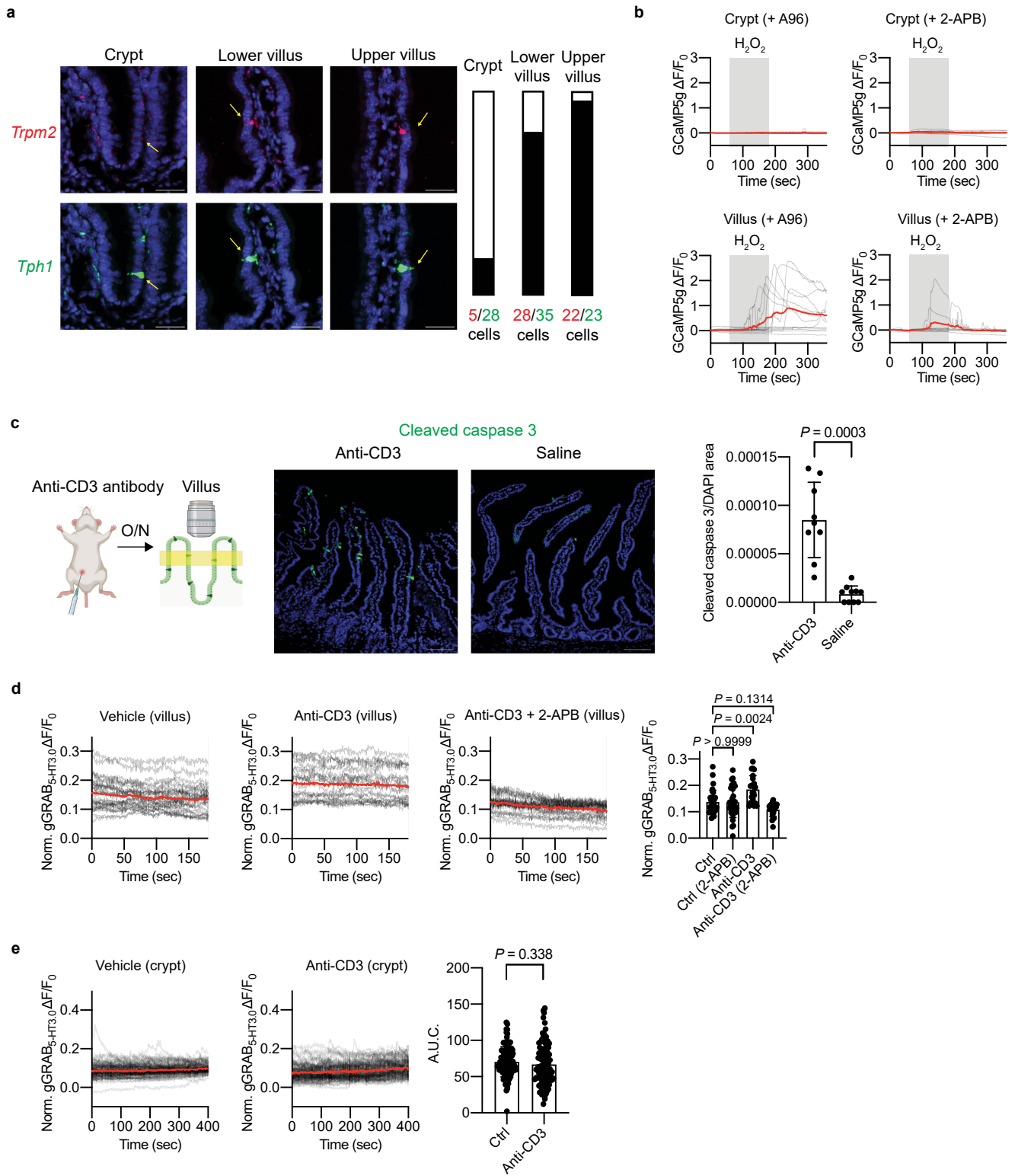
**Extended Data Fig. 5 | Visualization of 5-HT<sub>3</sub> receptor distribution and monitoring of serotonin transmission between EC cells and mucosal nerve fibres.** (a) Immunohistochemical labeling of HEK cells transiently transfected with 5-HT<sub>3A</sub>. Transfected or untransfected HEK cells were stained with VHH15-mCherry. Scale bar = 100  $\mu$ m. (b) Immunohistochemical labeling of 5-HT<sub>3</sub> receptors in the dorsal root ganglion (DRG: L5) myenteric plexus, and proximal colon with VHH15-mCherry. The signal was enhanced by staining for mCherry. Yellow arrows indicate cell bodies of *Htr3a*-EGFP(+) neurons in the myenteric plexus. Scale bar = 100  $\mu$ m for DRGs and 50  $\mu$ m for the myenteric plexus and proximal colon. (c) Three-dimensional rendering of EC cell (green), nerve fibres (purple), and basolateral membrane (red). (d) *Insm1*<sup>Cre</sup> labels both EC cells and mucosal nerves. EC cells were labeled with an anti-serotonin antibody and mucosal nerves were labeled with an anti-Tuj1 antibody. Yellow arrows indicate EC cells. Scale bar = 100  $\mu$ m. (e) Serotonin release and its propagation towards

mucosal nerve fibres in the crypts were visualized in ex vivo preparations. Simultaneous gGRAB<sub>5-HT3.0</sub> imaging of crypt EC cells and mucosal nerve fibres using *Insm1*<sup>Cre</sup>; *Rosa26*<sup>(gGRAB<sub>5-HT3.0</sub>-IP2A-JRGECO1a)</sup> mice. Crypts EC cells were stimulated by high K<sup>+</sup> (70 mM KCl) at the end of the recording. Blue and red arrows indicate EC cells and nerve fibres, respectively. Scale bar = 30  $\mu$ m, with each experiment repeated at least three times with similar results. (f) Serotonin release and its propagation towards mucosal nerve fibres in the villi were visualized in ex vivo preparations. Simultaneous gGRAB<sub>5-HT3.0</sub> imaging of villus EC cells (blue arrow) and nerve fibres (red arrow) using *Insm1*<sup>Cre</sup>; *Rosa26*<sup>(gGRAB<sub>5-HT3.0</sub>-IP2A-JRGECO1a)</sup> mice. Villus EC cells were electrically stimulated as indicated above the signal. Blue and red arrows indicate EC cells and nerve fibres, respectively. Scale bar = 10  $\mu$ m, with each experiment repeated at least three times with similar results.



**Extended Data Fig. 6 | Mucus limits the response of crypt EC cells to electrophiles.** (a) Electrophiles (100  $\mu\text{M}$ ) activate EC cells in *Tact1<sup>Cre</sup>; Polr2a<sup>(GCaMP5g-IRE5-tdTomato)</sup>* organoids. EC cells were stimulated by indicated electrophiles with (blue) and without (red) 100  $\mu\text{M}$  A96. (b) Dietary electrophiles

(100  $\mu\text{M}$ ) failed to activate crypt EC cells in the ex vivo preparations isolated from *Vill1<sup>Cre</sup>; Rosa26<sup>(gGRAB<sub>5-HT3.0</sub>-IP2A-JRGECO1a)</sup>* mice. (c) Electrophiles (100  $\mu\text{M}$ ) activated crypt EC cells after mucin digestion with StcE in the ex vivo preparations isolated from *Vill1<sup>Cre</sup>; Rosa26<sup>(gGRAB<sub>5-HT3.0</sub>-IP2A-JRGECO1a)</sup>* mice.

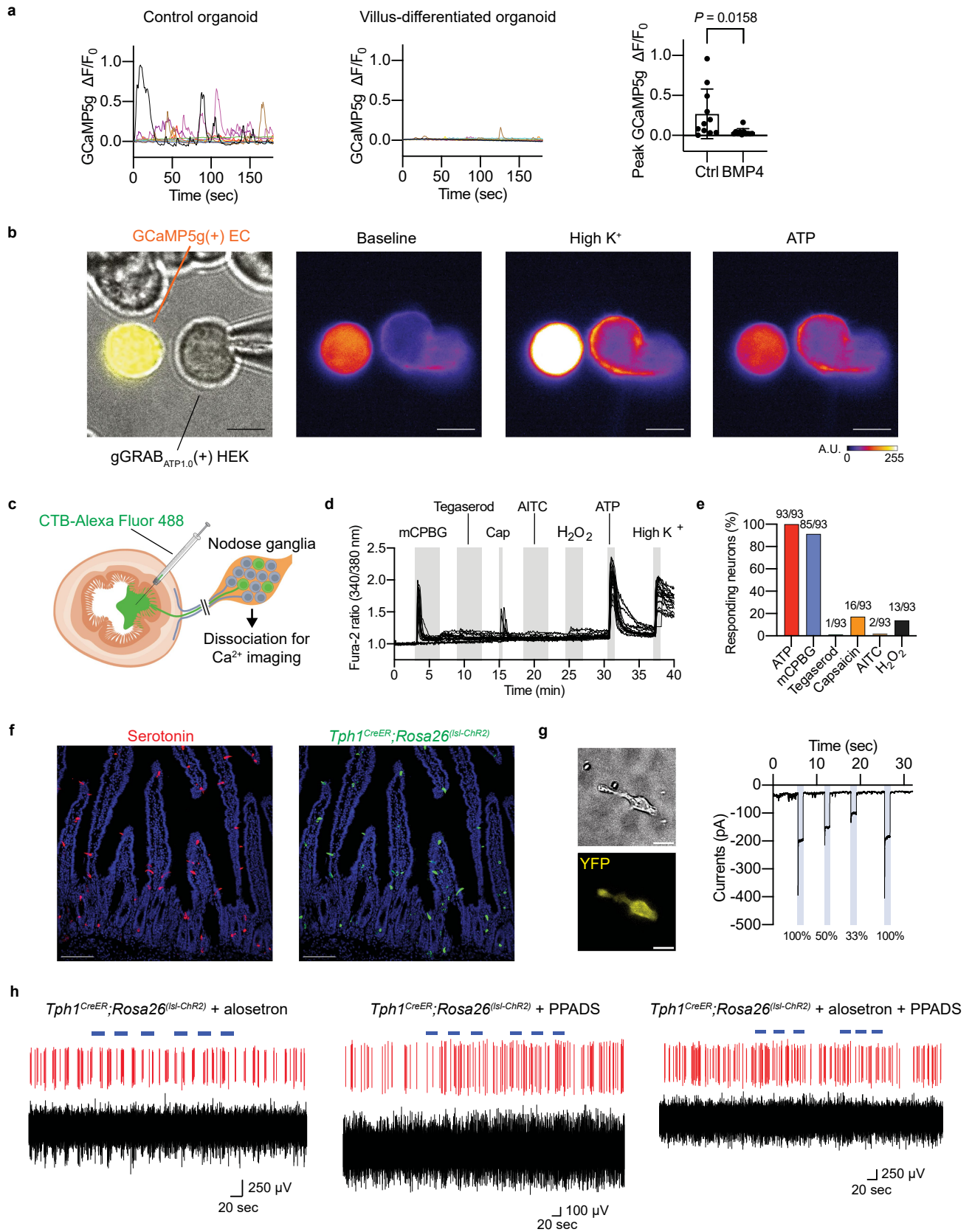


Extended Data Fig. 7 | See next page for caption.

**Extended Data Fig. 7 | Oxidative stress activates villus EC cells via TRPM2 channels.**

(a) In situ hybridization of *Trpm2* and *Tph1* in the small intestine. Yellow arrows indicate *Tph1*(+) EC cells. Bars indicate the ratio of *Trpm2*-positive cells/*Tph1*-positive cells. Quantification was performed using tissue samples from 3 independent animals. Scale bar = 30  $\mu$ m. (b) Oxidative stress activates villus EC cells. Dissociated EC cells expressing GCaMP5g were exposed to 200  $\mu$ M H<sub>2</sub>O<sub>2</sub> for 2 min in the presence or absence of 100  $\mu$ M A96 or 30  $\mu$ M 2-APB. (c) Anti-CD3 antibody induces epithelial cell apoptosis. Quantification of cleaved-caspase 3-positive cells (green) per DAPI area. Mean  $\pm$  s.d., two-sided Welch's t-test. n = 9 and 10 images per group. Scale bar = 100  $\mu$ m. (d) Anti-CD3 antibody-induced oxidative stress activates villus EC cells ex vivo.

The epithelial inflammation was induced by anti-CD3 antibody in serotonin sensor mice, and basal serotonin levels were measured in freshly isolated ex vivo prep in the presence or absence of 60  $\mu$ M 2-APB. Mean  $\pm$  s.d., two-way ANOVA with Tukey's multiple comparison test. n = 23–31 villi; N = 2–3 animals. (e) Oxidative stress does not activate crypt EC cells. The epithelial inflammation was induced by anti-CD3 antibody in gGRAB<sub>5-HT3.0</sub> mice, and basal serotonin levels were measured in freshly isolated ex vivo prep. gGRAB<sub>5-HT3.0</sub> was fully activated at the end of recordings for normalization. Mean  $\pm$  s.d., two-sided Welch's t-test. n = 100 crypts; N = 3 animals. The illustration in (c) was created using BioRender (<https://www.biorender.com>).

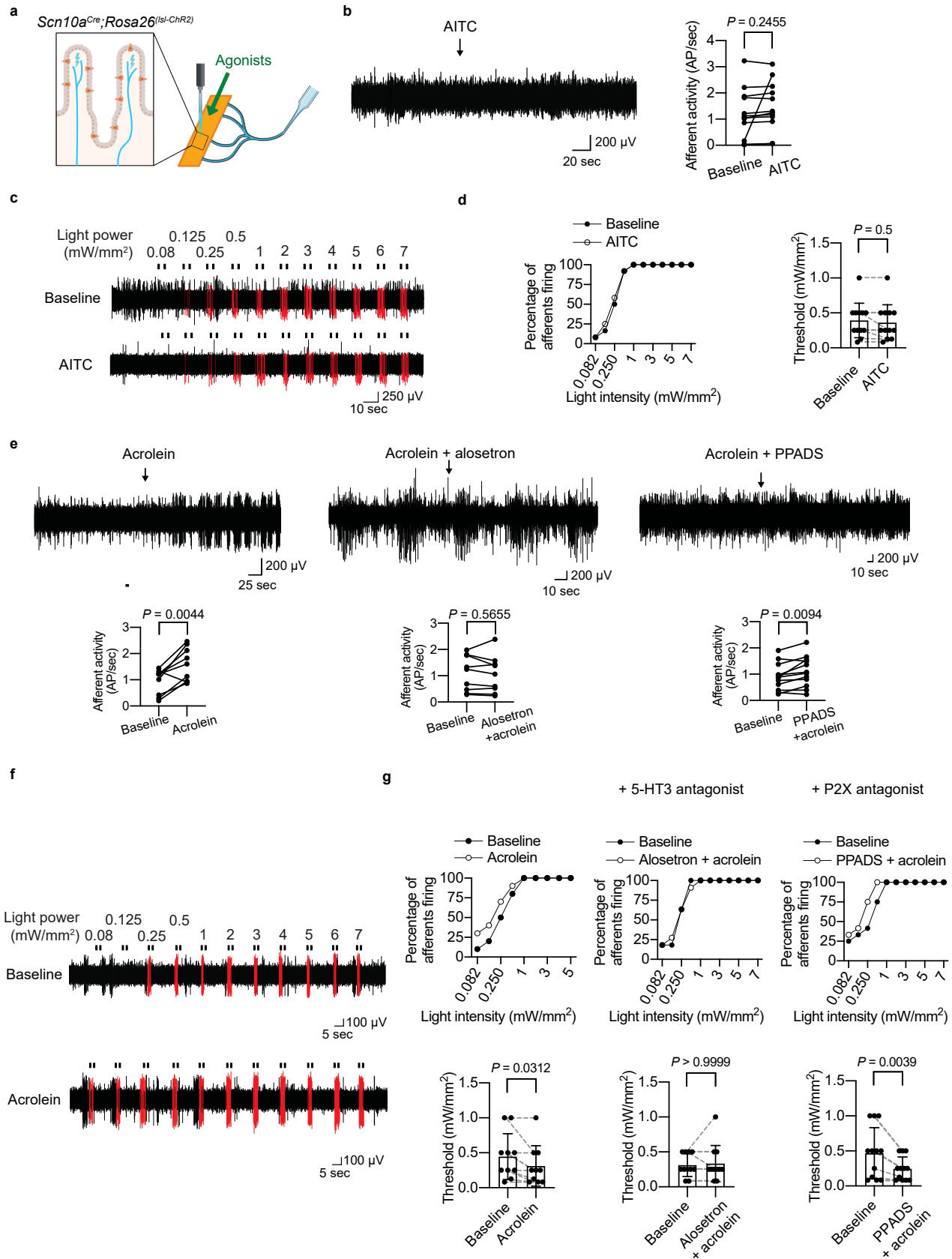


Extended Data Fig. 8 | See next page for caption.

**Extended Data Fig. 8 | Villus EC cells release ATP to activate mucosal sensory neurons.** (a) Spontaneous activity is diminished in villus-differentiated organoids. Peak GCaMP5g signal was compared between control and villus-differentiated organoids. Mean  $\pm$  s.d., two-sided Mann-Whitney U test.  $n = 11$  cells. (b) An example of ATP biosensor experiments. A HEK cell expressing the gGRAB<sub>ATP1.0</sub> sensor was positioned 5  $\mu\text{m}$  away from a single primary isolated GCaMP5g-expressing villus EC cell. The signals from the gGRAB<sub>ATP1.0</sub> sensor and GCaMP5g were simultaneously measured. EC cells were stimulated by high  $\text{K}^+$  (70 mM KCl). The gGRAB<sub>ATP1.0</sub> sensor was fully activated with 20  $\mu\text{M}$  ATP at the end of recordings for normalization. Scale bar = 10  $\mu\text{m}$ . (c) Green fluorescent-conjugated cholera toxin B (CTB) retrograde tracer was injected into the small intestine lumen to specifically trace mucosal afferents while excluding fibres innervating the muscle layer. The retrogradely traced vagal neurons were dissociated for calcium imaging. (d) Representative calcium imaging traces of dissociated small intestine mucosa-innervating vagal neurons. 10  $\mu\text{M}$  mCPBG (5-HT<sub>3</sub> agonist), 1  $\mu\text{M}$  tegaserod (5-HT<sub>4</sub> agonist), 50 nM capsaicin (TRPV1 agonist), 1  $\mu\text{M}$  AITC, 200  $\mu\text{M}$  H<sub>2</sub>O<sub>2</sub>, 10  $\mu\text{M}$  ATP, and 40 mM KCl (high  $\text{K}^+$ ) were applied as indicated above the signals. (e) The percentage of small intestine

mucosa-innervating vagal neurons responding to the applied agonists.  $n = 93$  neurons;  $N = 4$  animals. (f) Immunohistochemical labeling of EC cells in *Tph1<sup>CreER</sup>;Rosa26<sup>(1st-ChR2)</sup>* mice. This reporter line expresses the ChR2-YFP fusion protein. Serotonin and ChR2-YFP were immunostained with an anti-serotonin (red) and anti-GFP (green) antibodies. 70% (59 ChR2-YFP+ cells/84 serotonin+ cells) and 47% (31 ChR2-YFP+ cells/54 serotonin+ cells) of EC cells were labeled by YFP in villi and crypts, respectively. Scale bar = 100  $\mu\text{m}$ . (g) (Left) Representative image of dissociated ChR2-YFP-positive EC cells. Scale bar = 3  $\mu\text{m}$ . (Right) Light-activated inward currents in a dissociated EC cell. Various intensities of 470 nm laser stimulation were applied as indicated below the trace. The membrane potential was held at  $-80$  mV. (h) Representative jejunal afferent recordings during optogenetic stimulation of EC cells in the presence of, the 5-HT<sub>3</sub> antagonist (alosetron, 10  $\mu\text{M}$ ), the P2X antagonist (PPADS, 10  $\mu\text{M}$ ), or a combination of both antagonists (10  $\mu\text{M}$ ). The bottom black traces show the whole-nerve signal with multiple action potentials of different sizes and shapes. The red trace represents single-unit activity discriminated based on the spike waveform. The illustration in (c) was created using BioRender (<https://www.biorender.com>).

# Article

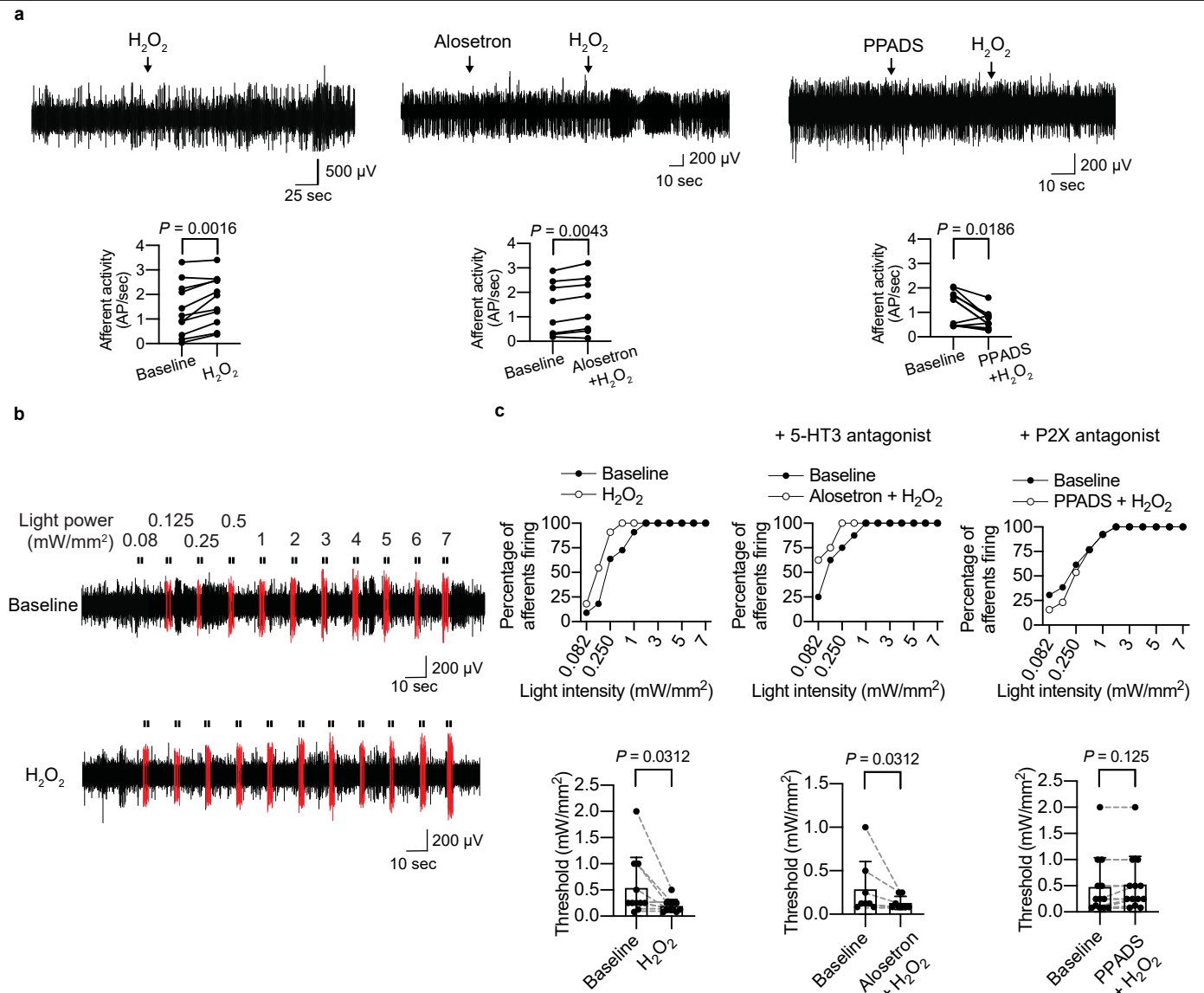


**Extended Data Fig. 9** | See next page for caption.

**Extended Data Fig. 9 | Crypt EC cells detect electrophiles and signal to mucosal sensory neurons through serotonergic transmission.**

(a) Schematic of ex vivo 'flat sheet' recordings from afferents innervating the jejunum of *Scn10a<sup>Cre</sup>;Rosa26<sup>(Isl-ChR2)</sup>* mice. TRPA1 or TRPM2 agonists were applied to the luminal surface. The illustration was created using BioRender.com. (b) Ex vivo recordings from jejunal afferents of *Scn10a<sup>Cre</sup>;Rosa26<sup>(Isl-ChR2)</sup>* mice. The number of action potentials is compared before and after application of 100  $\mu$ M AITC. Two-sided paired t-test. n = 12 recordings; N = 6 animals. (c) Representative jejunal mucosal afferent recordings with varying intensities of optogenetic stimulation of Na<sub>v</sub>1.8(+) nerve fibres in the absence or presence of 100  $\mu$ M AITC. Red signals represent light-evoked action potentials. (d) The percentage of afferents responding at indicated light intensities (left) and activation thresholds of jejunal afferents (right) before and after AITC treatment. Mean  $\pm$  s.d., Wilcoxon matched-pairs signed rank test. n = 12 recordings; N = 6 animals. (e) Ex vivo recordings from jejunal

afferents of *Scn10a<sup>Cre</sup>;Rosa26<sup>(Isl-ChR2)</sup>* mice. The number of action potentials/sec is compared before and after application of 100  $\mu$ M acrolein in the presence or absence of 10  $\mu$ M alosestron and 10  $\mu$ M PPADS. Two-sided paired t-test. Acrolein: n = 9 fibres; N = 4 animals. Alosestron + acrolein: n = 9 fibres; N = 5 animals. PPADS + acrolein: n = 12 fibres; N = 5 animals. (f) Representative jejunal afferent recordings with varying intensities of optogenetic stimulation of Na<sub>v</sub>1.8(+) nerve fibres in the absence or presence of 100  $\mu$ M acrolein. Red signals represent light-evoked action potentials. (g) The percentage of afferents responding at indicated light intensities (top) and activation thresholds of jejunal afferents (bottom) before and after acrolein treatment with or without 10  $\mu$ M alosestron and 10  $\mu$ M PPADS. Mean  $\pm$  s.d., Wilcoxon matched-pairs signed rank test. Acrolein: n = 10 recordings; N = 4 animals. Acrolein + alosestron: n = 11; N = 5. Acrolein + PPADS: n = 12 recordings; N = 5 animals. The illustration in (a) was created using BioRender (<https://www.biorender.com>).



**Extended Data Fig. 10 | Villus EC cells detect oxidative stress and signal to mucosal sensory neurons through purinergic transmission.** (a) Ex vivo recordings from jejunal afferents of *Scn10a<sup>Cre</sup>;Rosa26<sup>(ls1-ChR2)</sup>* mice. The number of action potentials/sec is compared before and after application of 200  $\mu$ M  $H_2O_2$  in the presence or absence of 10  $\mu$ M alossetron and 10  $\mu$ M PPADS. Two-sided paired t-test.  $H_2O_2$ ; n = 11 fibres; N = 4 animals. Alossetron +  $H_2O_2$ ; n = 8 fibres, N = 4 animals. Wilcoxon matched-pairs signed rank test: PPADS +  $H_2O_2$ ; n = 11 fibres, N = 4 animals. (b) Representative jejunal afferent recordings with

varying intensities of optogenetic stimulation of Na<sub>v</sub>1.8(+) nerve fibres in the absence or presence of 200  $\mu$ M  $H_2O_2$ . Red signals represent light-evoked APs. (c) The percentage of afferents responding at indicated light intensities (top) and activation thresholds of jejunal afferents (bottom) before and after  $H_2O_2$  treatment with or without 10  $\mu$ M alossetron and 10  $\mu$ M PPADS. Mean  $\pm$  s.d., Wilcoxon matched-pairs signed rank test.  $H_2O_2$ ; n = 11 recordings; N = 4 animals.  $H_2O_2$  + alossetron; n = 8 recordings; N = 4 animals.  $H_2O_2$  + PPADS; n = 13 recordings; N = 4 animals.

## Reporting Summary

Nature Portfolio wishes to improve the reproducibility of the work that we publish. This form provides structure for consistency and transparency in reporting. For further information on Nature Portfolio policies, see our [Editorial Policies](#) and the [Editorial Policy Checklist](#).

### Statistics

For all statistical analyses, confirm that the following items are present in the figure legend, table legend, main text, or Methods section.

n/a Confirmed

- The exact sample size ( $n$ ) for each experimental group/condition, given as a discrete number and unit of measurement
- A statement on whether measurements were taken from distinct samples or whether the same sample was measured repeatedly
- The statistical test(s) used AND whether they are one- or two-sided  
*Only common tests should be described solely by name; describe more complex techniques in the Methods section.*
- A description of all covariates tested
- A description of any assumptions or corrections, such as tests of normality and adjustment for multiple comparisons
- A full description of the statistical parameters including central tendency (e.g. means) or other basic estimates (e.g. regression coefficient) AND variation (e.g. standard deviation) or associated estimates of uncertainty (e.g. confidence intervals)
- For null hypothesis testing, the test statistic (e.g.  $F$ ,  $t$ ,  $r$ ) with confidence intervals, effect sizes, degrees of freedom and  $P$  value noted  
*Give  $P$  values as exact values whenever suitable.*
- For Bayesian analysis, information on the choice of priors and Markov chain Monte Carlo settings
- For hierarchical and complex designs, identification of the appropriate level for tests and full reporting of outcomes
- Estimates of effect sizes (e.g. Cohen's  $d$ , Pearson's  $r$ ), indicating how they were calculated

*Our web collection on [statistics for biologists](#) contains articles on many of the points above.*

### Software and code

Policy information about [availability of computer code](#)

#### Data collection

Immunofluorescence images of tissue sections and cells were captured on a Nikon CSU-W1 spinning disk confocal microscope run by the Micro-Manager software (v2.0). Immunofluorescence images of traced nodose ganglia and DRGs were captured on a Leica TCS SP8X laser scanning confocal microscope run by the Leica LAS software (v3.5.5.19976). GCaMP and serotonin sensor images were acquired through a Leica SP8 confocal microscope run by the LAS X software (v3.5.5.19976) or an upright microscope equipped with a Grasshopper 3 (FLIR) camera run by the Micro-Manager software (v2.0). Patch-clamp recordings were made by using a Digidata 1550B digitizer (Molecular Devices) connected to the pClamp software (v10.7). Short-circuit current ( $I_{sc}$ ) was measured using an EVC4000 multichannel voltage clamp (World Precision Instruments) connected to the pClamp software (v10.7). Calcium imaging of dissociated nodose neurons were made by using a Olympus IX71 microscope equipped with a CCD camera (Retiga ELECTRO). Nerve fiber recordings were made by using a 1401 interface (CED, Cambridge, UK) run by Spike2 software (V.5.18.).

#### Data analysis

We used the Fiji software (NIH, v2.14.) to generate maximal intensity projections and generate GCaMP and serotonin sensor deltaF/F images and traces. The Clampfit software (v11.2.2.17, Molecular Devices) was used to analyze patch-clamp recording data. The LabChart 8 software (AD Instruments) was used to analyze short-circuit current data. Immunofluorescence images were analyzed with Leica LAS Lite 4.0 (Leica Microsystems) or Fiji software v2.14 (NIH). Statistical analyses were done by using the Prism software (GraphPad, v8.4.3). Calcium imaging of dissociated neurons were analyzed using Metafluor software (Molecular Devices, V.7.8.0.0). Nerve fiber recordings were analyzed using Spike2 software (V.5.18). Published single-cell RNA sequencing datasets were analyzed with Seurat 5.0.1. on R 4.4.1

For manuscripts utilizing custom algorithms or software that are central to the research but not yet described in published literature, software must be made available to editors and reviewers. We strongly encourage code deposition in a community repository (e.g. GitHub). See the Nature Portfolio [guidelines for submitting code & software](#) for further information.

## Data

Policy information about [availability of data](#)

All manuscripts must include a [data availability statement](#). This statement should provide the following information, where applicable:

- Accession codes, unique identifiers, or web links for publicly available datasets
- A description of any restrictions on data availability
- For clinical datasets or third party data, please ensure that the statement adheres to our [policy](#)

All data generated or analyzed during this study are included in the manuscript (and its supplementary information data files).

## Research involving human participants, their data, or biological material

Policy information about studies with [human participants or human data](#). See also policy information about [sex, gender \(identity/presentation\), and sexual orientation](#) and [race, ethnicity and racism](#).

Reporting on sex and gender	N/A
Reporting on race, ethnicity, or other socially relevant groupings	N/A
Population characteristics	N/A
Recruitment	N/A
Ethics oversight	N/A

Note that full information on the approval of the study protocol must also be provided in the manuscript.

## Field-specific reporting

Please select the one below that is the best fit for your research. If you are not sure, read the appropriate sections before making your selection.

- Life sciences       Behavioural & social sciences       Ecological, evolutionary & environmental sciences

For a reference copy of the document with all sections, see [nature.com/documents/nr-reporting-summary-flat.pdf](https://www.nature.com/documents/nr-reporting-summary-flat.pdf)

## Life sciences study design

All studies must disclose on these points even when the disclosure is negative.

Sample size	For statistical comparisons, sample size was selected based on power calculations performed with reference to previous or present experiments carried out in our laboratory and in the field. For patch-clamp recording experiments, we collected data from 6-8 cells from 2-4 mice. For Ca2+ imaging experiments, we collected data from 8-13 cells from 2-3 mice. For biosensor experiments, we collected data from 8-9 cells from 8-9 organoids. For serotonin sensor imaging in mice, we collected data from 120-278 crypts and 10-31 villi from 2-4 mice. For BODIPY staining of tissues, we collected data from 9-21 crypt-villus in 3 mice. For organoid swelling assay, we collected data from 40-41 organoids. For Ussing chamber experiments, we collected data from 5-8 tissues from 3-4 mice. For calcium imaging of traced nodose neurons, we collected data from 92 neurons isolated from 4 mice. For RT-PCR of traced nodose neurons, we collected data from 25 neurons isolated from 4 mice. For nerve fiber recordings with Tph1-CreER;Isl-ChR2 mice, we collected data from 81-195 nerve fibers isolated from 33 Tph1-CreER;Isl-ChR2 and 4 Isl-ChR2 mice. For nerve fiber recordings with Nav1.8-Cre;Isl-ChR2 mice, we collected data from 8-12 jejunal afferents isolated from 4-6 animals.
Data exclusions	For Ca2+ imaging and serotonin sensor experiments, cells and tissues that showed substantial movements during imaging or abnormal high K+ responses, which indicate unhealthy cells and are commonly removed from data analysis, were not analyzed. For patch-clamp recording, we selected recordings that were made at an access resistance <15 MΩ and showed no drifting or excessive noise, which are common criteria for whole-cell patch-clamp recordings. As for the nerve fiber recordings, we excluded outliers based the Robust regression and Outlier removal (ROUT) method.
Replication	For patch-clamp recording, serotonin sensor imaging, biosensor experiments, and Ca2+ imaging experiments, we did not repeat the same stimulation on the same cell or tissue slice. Instead, we repeated the experiments on multiple cells or tissues from multiple animals and pooled the data for statistical analysis. All experiments involving multiple cohorts were routinely assessed on different days. Replication was successful on biosensor imaging, calcium imaging, patch-clamp recordings, afferent recordings, swelling assays, in situ hybridization, and immunohistological experiments.
Randomization	Genetically modified mice or control animals (littermates or age-matched mice) were randomly selected for histological, Ca2+ imaging, serotonin sensor imaging, afferent recordings, and patch-clamp recording experiments. For biosensor imaging, calcium imaging, and swelling assays, samples were randomly assigned to different drug treatment groups.

## Blinding

Where possible, experimenter was blinded from the genotype or drug treatment information when performing quantifications, including event counting, and intensity measurements.

## Reporting for specific materials, systems and methods

We require information from authors about some types of materials, experimental systems and methods used in many studies. Here, indicate whether each material, system or method listed is relevant to your study. If you are not sure if a list item applies to your research, read the appropriate section before selecting a response.

### Materials & experimental systems

n/a	Involvement	Involved in the study
<input type="checkbox"/>	<input checked="" type="checkbox"/>	Antibodies
<input type="checkbox"/>	<input checked="" type="checkbox"/>	Eukaryotic cell lines
<input checked="" type="checkbox"/>	<input type="checkbox"/>	Palaeontology and archaeology
<input type="checkbox"/>	<input checked="" type="checkbox"/>	Animals and other organisms
<input checked="" type="checkbox"/>	<input type="checkbox"/>	Clinical data
<input checked="" type="checkbox"/>	<input type="checkbox"/>	Dual use research of concern
<input checked="" type="checkbox"/>	<input type="checkbox"/>	Plants

### Methods

n/a	Involvement	Involved in the study
<input checked="" type="checkbox"/>	<input type="checkbox"/>	ChIP-seq
<input checked="" type="checkbox"/>	<input type="checkbox"/>	Flow cytometry
<input checked="" type="checkbox"/>	<input type="checkbox"/>	MRI-based neuroimaging

## Antibodies

### Antibodies used

Target and Conjugate, Host, Dilution, Manufacturer, Catalog #, RRID

#### Primary antibodies:

DsRed, Rabbit, 1:500, Takara Bio, 632496, AB\_10013483  
 GFP, Chicken, 1:500, Abcam, ab13970, AB\_300798  
 Serotonin, Rabbit, 1:1000, ImmunoStar, 20080, AB\_2313710  
 Tuj1, Rabbit, 1:1000, Abcam, ab18207, AB\_444319  
 Cleaved caspase 3, Rabbit, 1:500, Cell Signaling Technology, 9661, AB\_2341188  
 Lysozyme, rabbit, 1:1000, Agilent (Dako), EC 3.2.1.17, AB\_2341231

#### Secondary antibodies:

Rabbit IgG-Alexa Fluor 568, Donkey, 1:500, Thermo Fisher Scientific, A-10042, AB\_2534017  
 Rabbit IgG-Alexa Fluor 568, Goat, 1:500, Thermo Fisher Scientific, A-11036, AB\_10563566  
 Chicken IgY-Alexa Fluor 488, Goat, 1:500, Thermo Fisher Scientific, A-11039, AB\_2534096

### Validation

DsRed, Rabbit, 1:500, Takara Bio, 632496, AB\_10013483

Manufacturer's validation information: The antibody was tested by Western blot analysis. A specific band of approximately 30–38 kDa was observed in the lane loaded with lysate from cells expressing DsRed-Express. No band in this molecular weight range was detected for the lysates of the untransfected HEK 293 cells or the cells expressing AcGFP1.

Selected citations: PMID:35169021, PMID:35167440

GFP, Chicken, 1:500, Abcam, ab13970, AB\_300798

Manufacturer's validation information: This antibody is suitable for WB, ICC/IF

Selected citations: PMID: 34463618, PMID: 34292151

Serotonin, Rabbit, 1:1000, ImmunoStar, 20080, AB\_2313710

Manufacturer's validation information: The ImmunoStar Serotonin antiserum was quality control tested using standard immunohistochemical methods. The antiserum demonstrates significant labeling of rat hypothalamus, raphe nuclei and spinal cord using indirect immunofluorescent and biotin/avidin-HRP techniques. Staining is completely eliminated by pretreatment of the diluted antibody with 25 µg of serotonin/BSA. Cross reactivity of Serotonin antisera was examined. With 5 µg, 10 µg and 25 µg amounts the following substances did not react with diluted Serotonin antisera using the Bn-SA/HRP labeling method: 5-hydroxytryptophan, 5-hydroxyindole -3- acetic acid, and dopamine.

Selected citations: PMID: 28648659, PMID: 36949192

Tuj1, Rabbit, 1:1000, Abcam, ab18207, AB\_444319

Manufacturer's validation information: This antibody is suitable for ICC/IF, Flow Cyt (Intra), IHC-P, and WB.

Selected citations: PMID: 35794374, PMID: 36631663

Cleaved caspase 3, Rabbit, 1:500, Cell Signaling Technology, 9661, AB\_2341188

Manufacturer's validation information: Cleaved Caspase-3 (Asp175) Antibody detects endogenous levels of the large fragment (17/19 kDa) of activated caspase-3 resulting from cleavage adjacent to Asp175. This antibody does not recognize full length caspase-3 or other cleaved caspases. This antibody detects non-specific caspase substrates by western blot. Non-specific labeling may be observed by immunofluorescence in specific sub-types of healthy cells in fixed-frozen tissues (e.g. pancreatic alpha-cells). Nuclear background may be observed in rat and monkey samples.

Selected citations: PMID: 38629504, PMID: 38125299

Lysozyme, Rabbit, 1:1000, Agilent (Dako), EC 3.2.1.17, AB\_2341231

Manufacturer's validation information: Anti-human Lysozyme EC 3.2.1.17 antibodies. Applicable in the study of primary and secondary granules of myeloid cells. Produced under GMP standards. Strong batch-to-batch consistency. Analyte specific reagent for professional users.  
Selected citations: PMID: 35728595, PMID:34496236

## Eukaryotic cell lines

Policy information about [cell lines and Sex and Gender in Research](#)

Cell line source(s)	HEK293FT (Thermo Fisher Scientific, R70007) This line is derived from the 293F Cell Line (originally obtained from Robert Horlick at Pharmacoepia) and stably expresses the SV40 large T antigen from the pCMVSPORT6TAg.neo plasmid.  R-spondin 1 expressing HEK293T (Sigma, SCC111) This line is derived from the 293T cell line and stably expresses RSPO1, a protein used to establish 3D intestinal organoids.
Authentication	No authentication information could be found from the vendor's website
Mycoplasma contamination	No information about Mycoplasma contamination test could be found from the vendor's website
Commonly misidentified lines (See <a href="#">ICLAC</a> register)	N/A

## Animals and other research organisms

Policy information about [studies involving animals](#); [ARRIVE guidelines](#) recommended for reporting animal research, and [Sex and Gender in Research](#)

Laboratory animals	We used mice of both sexes between the age of 8-16 weeks. Mice were raised under regular diurnal (12:12) light-dark cycles at a temperature of 68-79 degrees F and a humidity of 30-70% with ad libitum access to food and water. Strains/genotypes used include:  Villin-Cre mice (MGI:2448639) from Jackson Laboratory Tac1-IRES-Cre mice (MGI:5484668) from Jackson Laboratory Insm1-GFP-Cre line (MGI:5576022) is a gift from Dr. Corey Harwell, UCSF. ePet1-Flp line (MGI:3795206) is a gift from Dr. Susan Dymecki, Harvard Medical School. Pirt1-Cre line (MGI:6332952) is a gift from Dr. Xinzhong Dong, Johns Hopkins Medicine. Polr2aGCaMP5G-tdTomato mice (MGI: 5560331) from Jackson Laboratory. Rosa26LSL-tdTomato mice (MGI: 3813512) from Jackson Laboratory. FL-hM3Dq mice (MGI:5771695) from Jackson Laboratory. Htr3a-GFP mice (MGI:5905283) is a gift from Dr. Massimo Scanziani, UCSF. Tph1-CreER (MGI:7439062) is a gift from Dr. Juanita L. Merchant, University of Arizona College of Medicine. Ai32(RCL-ChR2(H134R)/EYFP) (MGI:5013789) from Jackson Laboratory. Nav1.8-Cre was gifted from Dr. Wendy Imlach, Monash University, Australia. Jackson Laboratory, Strain no. 036564.  gGRAB5HT3.0-P2A-JRGECO1a mice were generated in this study.
Wild animals	The study did not involve wild animals.
Reporting on sex	We used mice of both sexes and pooled the data for analyses. No sex-based analyses were done as this is beyond the current scope of the study.
Field-collected samples	The study did not involve samples collected from the field.
Ethics oversight	All animal experiments done in UCSF were conducted in accordance with protocol AN192533 approved by the Institutional Animal Care and Use Committee, University of California – San Francisco. All animal experiments done in South Australian Health and Medical Research Institute (SAHMRI) were approved and performed in accordance with the guideline of the Animal Ethics Committees of SAHMRI.

Note that full information on the approval of the study protocol must also be provided in the manuscript.

## Plants

### Seed stocks

*Report on the source of all seed stocks or other plant material used. If applicable, state the seed stock centre and catalogue number. If plant specimens were collected from the field, describe the collection location, date and sampling procedures.*

### Novel plant genotypes

*Describe the methods by which all novel plant genotypes were produced. This includes those generated by transgenic approaches, gene editing, chemical/radiation-based mutagenesis and hybridization. For transgenic lines, describe the transformation method, the number of independent lines analyzed and the generation upon which experiments were performed. For gene-edited lines, describe the editor used, the endogenous sequence targeted for editing, the targeting guide RNA sequence (if applicable) and how the editor was applied.*

### Authentication

*Describe any authentication procedures for each seed stock used or novel genotype generated. Describe any experiments used to assess the effect of a mutation and, where applicable, how potential secondary effects (e.g. second site T-DNA insertions, mosaicism, off-target gene editing) were examined.*